The mechanical power output of the flight muscles of blue-breasted quail (*Coturnix chinensis*) during take-off

Graham N. Askew[1,*], Richard L. Marsh[2] and Charles P. Ellington[1]

[1]*Department of Zoology, Downing Street, University of Cambridge, Cambridge CB2 3EJ, UK* and [2]*Department of Biology, Northeastern University, 360 Huntington Avenue, Boston, MA 02115, USA*

*Author for correspondence at present address: School of Biology, University of Leeds, Leeds LS2 9JT, UK (e-mail: g.n.askew@leeds.ac.uk)

Summary

Blue-breasted quail (*Coturnix chinensis*) were filmed during take-off flights. By tracking the position of the centre of mass of the bird in three dimensions, we were able to calculate the power required to increase the potential and kinetic energy. In addition, high-speed video recordings of the position of the wings over the course of the wing stroke, and morphological measurements, allowed us to calculate the aerodynamic and inertial power requirements. The total power output required from the pectoralis muscle was, on average, 390 W kg^{-1}, which was similar to the highest measurements made on bundles of muscle fibres *in vitro* (433 W kg^{-1}), although for one individual a power output of 530 W kg^{-1} was calculated. The majority of the power was required to increase the potential energy of the body. The power output of these muscles is the highest yet found for any muscle in repetitive contractions.

We also calculated the power requirements during take-off flights in four other species in the family Phasianidae.

Power output was found to be independent of body mass in this family. However, the precise scaling of burst power output within this group must await a better assessment of whether similar levels of performance were measured across the group. We extended our analysis to one species of hawk, several species of hummingbird and two species of bee. Remarkably, we concluded that, over a broad range of body size (0.0002–5 kg) and contractile frequency (5–186 Hz), the myofibrillar power output of flight muscles during short maximal bursts is very high (360–460 W kg^{-1}) and shows very little scaling with body mass. The approximate constancy of power output means that the work output varies inversely with wingbeat frequency and reaches values of approximately 30–60 J kg^{-1} in the largest species.

Key words: blue-breasted quail, *Coturnix chinensis*, power output, take-off, aerodynamics.

Introduction

Understanding the limits of performance of skeletal muscle requires an integrated approach that examines organismal performance as well as the physiological properties of the muscles used. The power output of skeletal muscle during locomotion is very sensitive to the details of the strain cycle (Askew and Marsh, 1997; Askew and Marsh, 1998; Askew and Marsh, 2001). The strain cycle is determined by the interaction between the active muscles and the load upon which they act. These loads *in vivo* are not fixed, but instead are determined by the interaction between morphological structures of the animal and the environment through which the animal is moving (Marsh, 1999). In understanding the factors that favour high power output, it is helpful to focus our integrative efforts on systems that have evolved to produce high power output. One such system is the avian locomotor system involved in flight. As opposed to terrestrial locomotion, during which muscles with quite differing functions operate together (Marsh, 1999), flight requires that the major muscular effort be directed to producing mechanical power (Biewener, 1998).

Estimates of the power required to fly have been central in understanding the morphological adaptations, limitations and evolution of animal flight. A number of methods have been used to estimate the power output required from the flight muscles of insects and flying vertebrates, both extinct and extant. Both theoretical methods, based on lifting-line, blade element or free vortex theory, and experimental methods, based on *in vivo* and *in vitro* measurements of muscle power output, flow visualisation and kinematics, have been used (Pennycuick, 1968; Pennycuick, 1969; Weis-Fogh, 1972; Rayner, 1979; Rayner, 1995; Ellington, 1984; Biewener et al., 1992; Dial and Biewener, 1993; Biewener et al., 1998; Josephson, 1985; Josephson et al., 2000; Spedding, 1986; Spedding, 1987; Spedding et al., 1984; Pennycuick et al., 2000).

In the preceding paper (Askew and Marsh, 2001), we described experiments performed on blue-breasted quail (*Coturnix chinensis*) in which we measured the power output of the pectoralis muscle *in vitro*. Sonomicrometry and electromyography (EMG) were used to determine the strain and

activity patterns of the muscle during take-off and horizontal flights. Using bundles of muscle fibres isolated from the pectoralis, we replicated the *in vivo* operating conditions of the pectoralis muscle *in vitro* using the work loop technique (Josephson, 1985). The net power output generated during shortening and averaged over the whole wing stroke was approximately $350\,\mathrm{W\,kg^{-1}}$, with several preparations generating over $400\,\mathrm{W\,kg^{-1}}$ and the highest measured for one preparation of $433\,\mathrm{W\,kg^{-1}}$. These estimates of power output exceed by a considerable margin other estimates so far available for avian flight muscles based on *in vivo* measurements or calculations.

The present study evaluates whether the high values obtained from *in vitro* pectoralis muscle preparations are consistent with the performance of quail during take-off flight. We estimated the power required from the pectoralis muscle on the basis of the movement of the centre of mass of the bird and aerodynamic analysis. Quail were filmed during take-off to determine their flight trajectory in three dimensions, allowing changes in potential and kinetic energy to be determined. In addition, high-speed video was used to record the wing kinematics, which were used to estimate the inertial and aerodynamic power requirements.

Materials and methods

Flight chamber and filming

Two screens, marked with a $5\,\mathrm{cm}$ square grid, were placed perpendicular to each other to form a calibrated filming arena (Fig. 1). A mist net was used to enclose the other sides and the top of the flight chamber. Two video cameras recording at $60\,\mathrm{fields\,s^{-1}}$ (Panasonic S-VHS Reporter with an 8–80 mm zoom lens and Sony Video Hi8 Handy Cam with an 11–88 mm zoom lens) were placed on tripods oriented normal to the calibration screens. These cameras allowed the position of the bird to be tracked in three dimensions. A NAC colour high-speed video camera recording at $500\,\mathrm{fields\,s^{-1}}$ was suspended above and looking down into the flight chamber, allowing the kinematics of the wing stroke to be recorded. The two 60 Hz-cameras were shuttered at $1\,\mathrm{ms}$, and the high-speed camera was shuttered at $0.4\,\mathrm{ms}$. Illumination was provided by $3400\,\mathrm{W}$ of lighting placed above and to the sides of the flight chamber. A computer-generated signal was used to light a light-emitting diode, which was recorded in the view of both 60 Hz cameras. This allowed the images from both of these cameras to be synchronized.

For the take-off flights, the bird was placed in a covered cardboard cylinder on top of a wire cage. To induce flight, the lid was removed from the cylinder, and the bird was encouraged from below.

Sonomicrometry

To correlate the position of the wings with the strain cycle of the pectoralis, we implanted sonomicrometry crystals into the pectoralis muscle in some of the quails. Sonomicrometry allows strain to be estimated by measuring the transit time of ultrasonic sound waves from a transmitter crystal to a receiver crystal [for further details, see Askew and Marsh (Askew and Marsh, 2001)].

Muscle length (L) data was sampled at a frequency of $1050\,\mathrm{Hz}$ using the acquisition software SonoLAB (Sonometrics Corporation, London, Canada) running on a 486DX personal computer. The resting length of the muscle (L_R) was defined as the mean muscle length in the period prior to take-off, corrected for the crystal holder offset (Askew and Marsh, 2001). Strain was calculated as $(L–L_R)/L_R$. The velocity of sound in muscle was assumed to be $1540\,\mathrm{m\,s^{-1}}$ (Griffiths, 1987).

Film analysis

All recordings were initially assessed to determine which flights to analyse. A flight was analysed if the bird took off vertically and flew without colliding with the sides of the flight chamber. Using the synchronized images from the two normal-speed video cameras, the position of the bird (taken as the centre of the body) was determined using an x, y, z coordinate system; x and y are orthogonal coordinates in the horizontal plane, and z is the vertical coordinate (Fig. 1). These coordinates represent the apparent position of the bird and had to be corrected for parallax to give the actual position.

The angle between the origin and the bird is given by $\delta',\varepsilon',\phi'$ in the y, x and z directions, respectively, and is calculated using the following equations:

$$\delta' = \tan^{-1}\left(\frac{y_{\max}}{2A}\right) - \tan^{-1}\left(\frac{y_{\max}}{2A} - \frac{y_{\mathrm{im}}}{A}\right), \qquad (1)$$

$$\varepsilon' = \tan^{-1}\left(\frac{x_{\max}}{2B}\right) - \tan^{-1}\left(\frac{x_{\max}}{2B} - \frac{x_{\mathrm{im}}}{B}\right), \qquad (2)$$

$$\phi' = \tan^{-1}\left(\frac{z_{\max}}{2A}\right) - \tan^{-1}\left(\frac{z_{\max}}{2A} - \frac{z_{\mathrm{im}}}{A}\right), \qquad (3)$$

where A and B are the distances between the optical centre of the camera lens and the screen for each of the two cameras (4.78 and $4.15\,\mathrm{m}$, respectively), $x_{\max}$, $y_{\max}$ and $z_{\max}$ are the dimensions of the field of view in each of the respective axes, and x_{im}, y_{im} and z_{im} are the distances between the origin and the image of the bird in each of the respective axes (see Fig. 1).

The 'real' x, y and z coordinates were calculated by trigonometry using the equations:

$$x = \frac{x_{\mathrm{im}} + y_{\mathrm{im}} \tan\left(\dfrac{\varepsilon}{2} - \varepsilon'\right)}{1 - \tan\left(\dfrac{\delta}{2} - \delta'\right)\tan\left(\dfrac{\varepsilon}{2} - \varepsilon'\right)}, \qquad (4)$$

$$y = y_{\mathrm{im}} + x \tan\left(\frac{\delta}{2} - \delta'\right), \qquad (5)$$

$$z = z_{\mathrm{im}} - x \tan\left(\frac{\phi}{2} - \phi'\right), \qquad (6)$$

where δ, ε and ϕ are the opening angles of the camera in the y, x and z directions, respectively (Fig. 1).
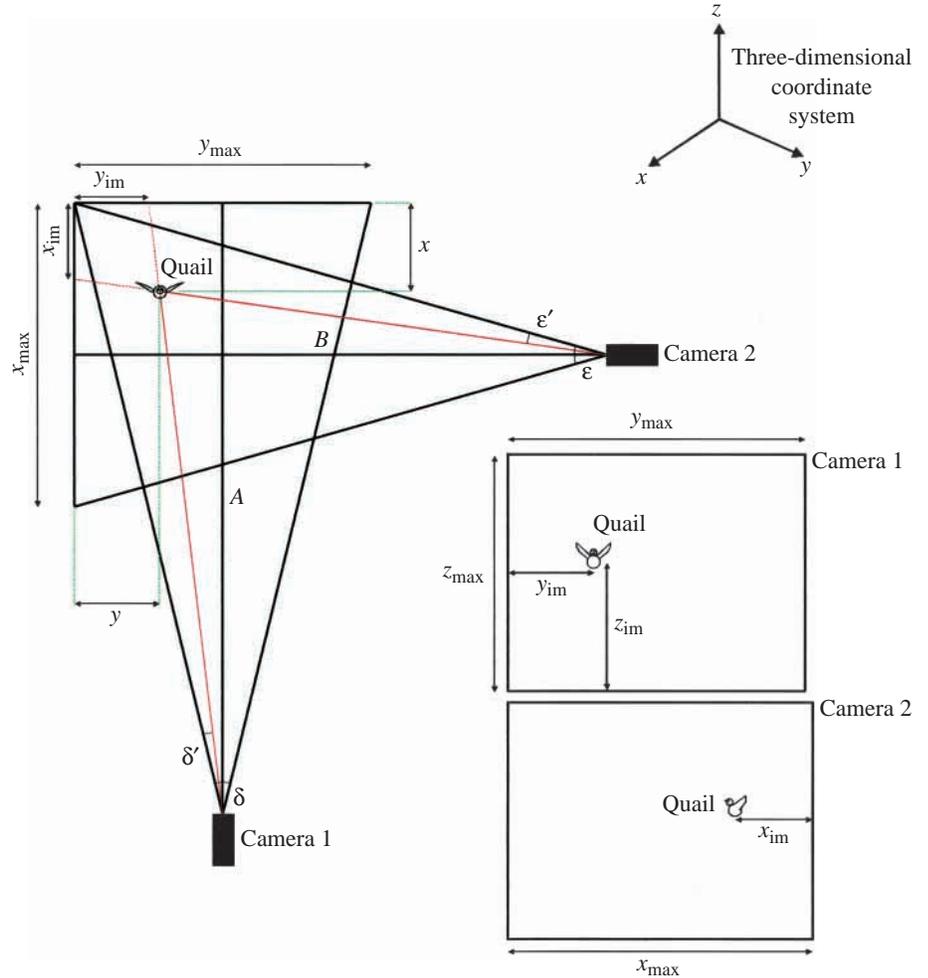
Fig. 1. Two-dimensional representation of the filming arena used to record the movements of the centre of mass of the quail during take-off. Two cameras were positioned normally at a distance A and B, respectively, from two calibrated screens. The two images recorded in the two cameras had dimensions represented by x_{max}, y_{max} and z_{max}, according to a right-handed three-dimensional coordinate system. The position of the centre of mass of the quail in the camera images was defined by the coordinates x_{im}, y_{im} and z_{im}. The 'real' coordinates of the quail were calculated by correcting for parallax using equations 1–6. δ, ε, opening angles of the cameras; δ', ε', angles between the bird and the origin.

Velocity of the centre of mass and mean power output

The x, y and z coordinates of the centre of mass of the birds were plotted with respect to time for each flight, and quadratic and cubic equations were fitted to the data. Only flights in which acceleration was constant, i.e. the r^2 values for the quadratic and cubic equations were similar (Wakeling and Ellington, 1997a), were used for further analysis. Fig. 2 shows three-dimensional positional data for a typical flight. Velocities ($\dot{x}$, $\dot{y}$ and $\dot{z}$) were estimated by differentiating the quadratic equation in each axis dimension, and the overall velocity (v) of the bird's centre of mass was calculated as follows:

$$v = \sqrt{\dot{x}^2 + \dot{y}^2 + \dot{z}^2} . \tag{7}$$

The angle of elevation (χ) of the flight path with respect to the horizontal was calculated as:

$$\chi = \tan^{-1}\left(\frac{\dot{z}}{\sqrt{\dot{x}^2 + \dot{y}^2}}\right). \tag{8}$$

The mean rate of change in the kinetic energy ($E_{K,ext}$) and potential energy (E_P) of the centre of mass of the bird was estimated over the entire flight:

$$\frac{dE_{K,ext}}{dt} = \frac{M_b}{2} \frac{(v_{max}^2 - v_{min}^2)}{\Delta t}, \tag{9}$$

$$\frac{dE_P}{dt} = M_b g \dot{z} , \tag{10}$$

where M_b is the body mass, v_{max} and v_{min} are the maximum and minimum velocity, respectively, g is gravitational acceleration and Δt is the flight duration. Note that v_{min} is not zero because the bird is already moving before it is visible above the cardboard cylinder in which the flight is initiated. Thus, we did not include the initial acceleration of the bird upwards, which is partly powered by leg muscles as the bird jumps into the air (Earls, 2000). In flights in which the bird decelerated, the rate of change of kinetic energy was defined as being negative.

Wing mass and area distribution

The wing from a freshly killed quail was carefully removed at the shoulder joint and pinned out in an extended position as observed in mid-downstroke. The wing was photographed, and the image was scanned into a computer. Using Scion Image, the image of the wing was divided into 11 strips of equal width,

A
$x=5.1t^2-0.67t+0.38$ $(r^2=0.995)$
$y=-0.92t^2+0.78t+0.39$ $(r^2=0.971)$
$z=1.08t^2+4.2t+0.044$ $(r^2=0.997)$
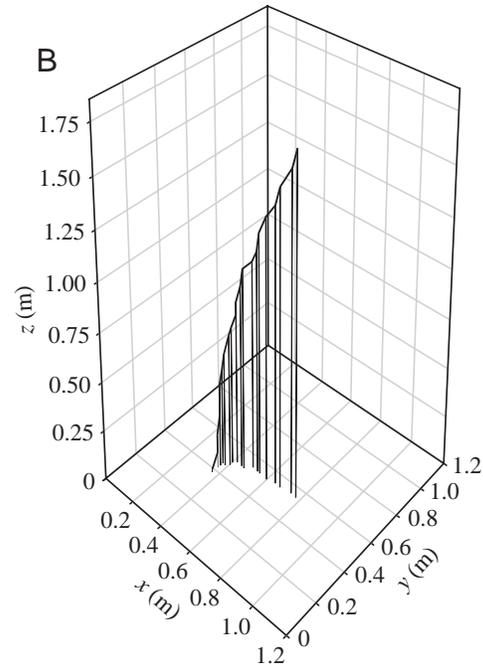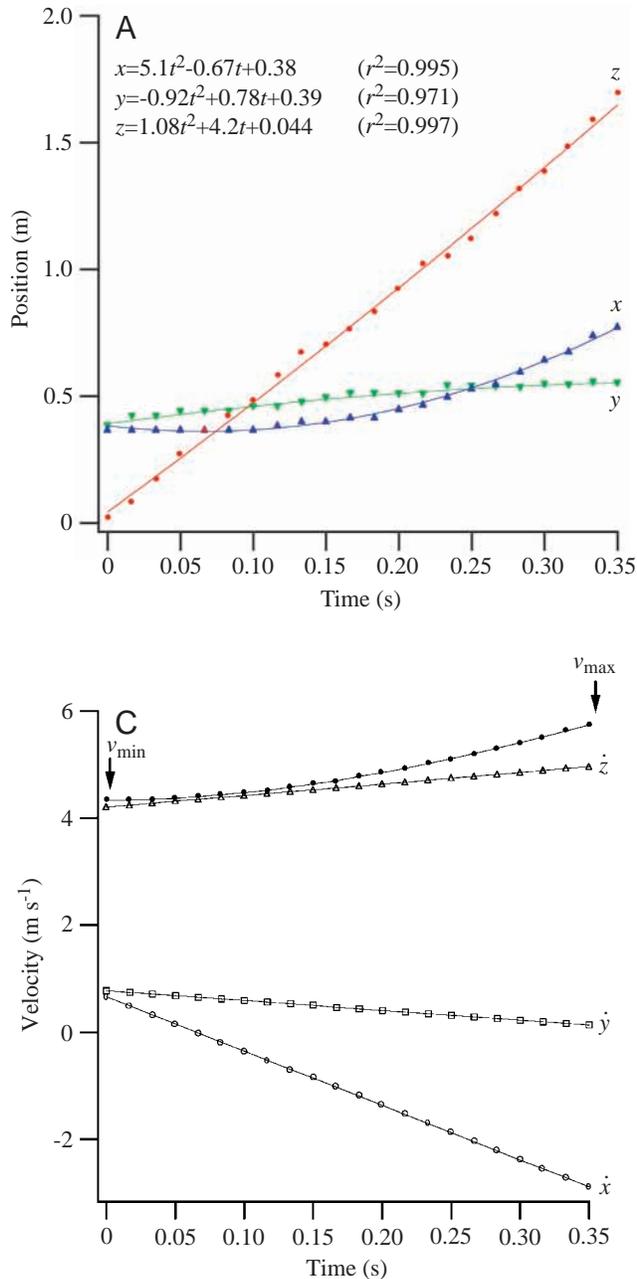
Fig. 2. (A) Two-dimensional representation of a typical take-off flight in a quail, for the three coordinates describing its three-dimensional position (x, y and z), plotted with respect to time (t). Quadratic equations have been fitted to the position data, and the r^2 values for these are shown. (B) Three-dimensional representation of the flight illustrated in A. The axes have been scaled such that they represent the size of the flight chamber. (C) Velocity of the centre of mass of the quail during take-off for the flight illustrated in A and B. The initial velocity of the bird (v_{min}) was $4.33\,\mathrm{m\,s^{-1}}$, and velocity increased to a maximum of $5.74\,\mathrm{m\,s^{-1}}$ (v_{max}) by the end of the flight. The rate of change of kinetic energy of the body was calculated using equation 9:

$$\frac{dE_{K,ext}}{dt} = \frac{0.043}{2} \times \frac{(5.74^2-4.33^2)}{0.35} = 0.31\,\mathrm{W}.$$

The initial kinetic energy of the body is deducted in this calculation because at least some proportion of this may be contributed by the hindlimbs. $\dot{x}$, $\dot{y}$, $\dot{z}$, velocity of the centre of mass in the x, y and z directions, respectively.

perpendicular to the wing axis, and the area of each strip was determined.

The wing was cut into 11 strips, as described above, and each strip was weighed to determine the distribution of mass from base to tip. The mass and area of each strip were calculated as a proportion of that for the whole wing and were assumed to be representative of all the quails used in this study. The proximal and middle wing were represented by two strips each, with the remaining strips occurring in the distal region of the wing.

Induced power requirements for climbing flight

To provide a vertical force, the wings must impart downward momentum to air in the wake. The corresponding downwash, or induced velocity w, can be determined using classical actuator disc theory from the momentum flux of air required to balance the weight and any vertical acceleration force. The actuator disc represents the swept area over which the wings interact with the air and was calculated from the detailed wing kinematics. The induced velocity at the level of the actuator disc for vertical, accelerating flight is given by Wakeling and Ellington (Wakeling and Ellington, 1997b) as:

$$w = -\frac{\dot{z}}{2} + \sqrt{\frac{\dot{z}^2\rho D + 2M_b(\boldsymbol{g}+\ddot{z})}{4\rho D}}, \tag{11}$$

where ρ is air density (taken as $1.2\,\mathrm{kg\,m^{-3}}$), $\dot{z}$ is the vertical velocity of the bird, $\ddot{z}$ is the vertical acceleration of the bird

(both positive upwards), and D is the area of the actuator disc. In classical actuator disc theory, the induced velocity is considered to be steady and constant over the disc area and, hence, it is the absolute minimum value that satisfies the momentum flux requirement. For a more realistic estimate of the induced velocity, this value is multiplied by a correction factor k, usually taken as 1.2 (Ellington, 1984).

The actuator disc therefore generates a vertical force $M_b(\boldsymbol{g}+\ddot{z})$ by imparting an induced velocity kw to air entering the disc with vertical velocity $\dot{z}$. The rate at which work is done by the disc, conventionally called the induced power P_{ind}, is equal to this force multiplied by the total air velocity, $kw+\dot{z}$:

$$P_{ind} = M_b(\boldsymbol{g} + \ddot{z})(kw + \dot{z}) = M_b kw(\boldsymbol{g} + \ddot{z}) + M_b \boldsymbol{g}\dot{z} + M_b \ddot{z}\dot{z}. \quad (12)$$

The far right-hand-side of this equation clearly shows how the work is partitioned. The term $M_b \boldsymbol{g}\dot{z}$ is the rate of increase of potential energy of the body, and the term $M_b \ddot{z}\dot{z}$ is the rate of increase of kinetic energy; it should be noted that any work done in changing the potential and kinetic energy of the body must be reflected in the kinetic energy of the wake. These quantities have already been calculated in equation 9 and equation 10 independently from the movement of the centre of mass, so we need only calculate the contribution of the first term to the induced power. This is the induced power required to generate the induced velocity *per se*, which shall be denoted by a prime:

$$P_{ind}' = M_b kw(\boldsymbol{g} + \ddot{z}). \quad (13)$$

Parasite power

Parasite power (P_{par}), the power required to overcome drag on the body, is given by:

$$P_{par} = \frac{1}{2} \rho S_b C_{D,par} v^3, \quad (14)$$

where S_b is the frontal area of the body, $C_{D,par}$ is the drag coefficient of the body and v is the speed of the centre of mass of the bird (Pennycuick et al., 1988). Values for $C_{D,par}$ vary widely in the literature and depend on Reynolds number (Re). In our experiments, Re was 16600. On the basis of measurements of the drag on frozen bird bodies, Pennycuick et al. (Pennycuick et al., 1988) proposed a relationship between $C_{D,par}$ and Re. For the Re used by quail during take-off, a value for $C_{D,par}$ of 0.4 should be used. More recently, however, Pennycuick et al. (Pennycuick et al., 1996) revised $C_{D,par}$ estimates on the basis of an observed discrepancy between the speed at which the minimum wingbeat frequency was observed and the calculated minimum power speed (v_{mp}). A $C_{D,par}$ value of 0.05 is suggested for an Re range of 21600–215000. However, Rayner (Rayner, 1999) suggests that the reduction in $C_{D,par}$ should be around one-third of the original values (rather than one-eighth as suggested by Pennycuick's new estimates), but that it decreases with speed. We use a $C_{D,par}$ of 0.13 in our calculations, as suggested by Rayner (Rayner, 1999). In any case, the parasite power is low compared with the other power components, so uncertainty about $C_{D,par}$ will have no significant effect on the total power output.

Profile power output

The mean profile power to overcome the pressure and friction drag acting on a wing strip i, averaged over the entire wing stroke, is given by:

$$P_{pro} = 2 \sum \left(\frac{1}{2} \rho V_{R,i}^3 S_i C_{D,pro} \right) \quad (15)$$

[modified from Norberg (Norberg, 1990)]. Note the factor of 2 to account for the two wings. S is the wing strip area, V_R is the resultant velocity of the wing strip and $C_{D,pro}$ is the profile drag coefficient. $C_{D,pro}$ was taken to be 0.02 (Rayner, 1979; Pennycuick et al., 1992).

V_R was calculated from the induced velocity (w), the upward velocity ($\dot{z}$) and the flapping velocity of each wing strip ($\omega_i r_i$) as follows:

$$V_R = \sqrt{(w + \dot{z} - \omega_i r_i \sin \varphi)^2 + (V_h + \omega_i r_i \cos \varphi)^2}, \quad (16)$$

where ω_i is the angular velocity of the wing strip with respect to the shoulder joint, r_i is the distance from the wing strip to the shoulder joint, φ is the angle of the stroke plane with respect to the horizontal and V_h is velocity of the bird in the horizontal plane. We were unable to measure φ, so we calculated V_R for φ ranging between 0 and 30°, which includes the stroke plane that has been measured in hovering pigeon (*Columba livia*), pied flycatcher (*Ficedula hypoleuca*), the long-eared bat (*Plecotus auritus*) and the bat *Glossophaga soricina* (Pennycuick, 1968; Norberg, 1975; Norberg, 1976; Norberg et al., 1993).

Inertial power requirements

High-speed video images of the bird during take-off were digitized (Scion Image) to enable the wing segment angles to be determined over the wing stroke. The wing of the quail moves in three segments, which we will term the proximal, middle and distal wing, separated by the elbow and wrist joints (Fig. 3). The proximal wing includes the humerus, which supports the tertials, the middle wing includes the radius and ulna, which support the secondaries, and the distal wing consists of the carpals and metacarpals, which support the primaries. The angles of each wing segment in the horizontal plane were determined from the video recordings and are represented by the angles α (proximal wing), β (middle wing) and γ (distal wing). Fourier series of the form:

$$\alpha_f, \beta_f, \gamma_f = \frac{a_0}{2} + \sum (a_n \cos nX + b_n \sin nX) \quad (17)$$

were fitted to the data, where α_f, β_f and γ_f are the Fourier-smoothed wing angles that represent the angles α, β and γ, respectively, a and b are the Fourier coefficients, n is the harmonic number and X is relative time ($-\pi$ to π). Up to five harmonics were calculated. The wing amplitude predicted by the Fourier series was compared with the raw data by calculating the standard error (S.E.M.):

Table 1. *Fourier coefficients for a series of four representative wing strokes from a quail during take-off*

	α				β				γ		
a_0	54.06			a_0	−14.18			a_0	−55.72		
a_1	44.65	b_1	56.91	a_1	−1.06	b_1	81.43	a_1	−30.50	b_1	93.09
a_2	10.01	b_2	−7.93	a_2	1.36	b_2	8.90	a_2	−7.40	b_2	17.57
a_3	−4.28	b_3	1.28	a_3	−1.83	b_3	−1.68	a_3	−2.35	b_3	−1.24
S.E.M.		8.50		S.E.M.		0.95		S.E.M.		7.48	

α, β and γ are the angles of the proximal, middle and distal wing segments, respectively, in the horizontal plane; a_0, a_1,...b_1, ..., b_3 are the Fourier coefficients (see equation 17).

S.E.M. is the standard error of the calculated wing segment amplitude compared with the observed amplitude (see equation 18).

$$\text{S.E.M.} = \sqrt{\frac{(O_i - E_i)^2}{N}}, \qquad (18)$$

where O is the observed data, E is the value predicted from the Fourier series, N is the number of data points and i is the data point number. Table 1 presents Fourier coefficients for a series of four representative wing strokes for a quail during take-off flight.

The inertia of the wing is increased by the mass of air that is accelerated with the wing. This is termed the virtual or added mass (m_v) and, for each wing strip, was calculated as:

$$m_v = \frac{1}{4} \pi \rho c^2 dr, \qquad (19)$$

where c is the mean chord of the strip (calculated as strip area divided by strip width) and dr is the strip width (Norberg, 1990).

The moment of inertia (I) of each wing strip about the shoulder joint was calculated from the total mass of the strip ($m_i + m_v$) and its distance from the shoulder joint r_i.

The kinetic energy of both wings ($E_{K,int}$) was calculated from the angular velocity of each strip (ω_i) and its moment of inertia (I_i) at each stage of the wing stroke:

$$E_{K,int} = 2 \sum_{i=1}^{11} \frac{1}{2} I_i \omega_i^2 . \qquad (20)$$

Note the factor of 2 to account for both wings.

Results

Morphological data for the quail whose flights were analysed are given in Table 2. The mean mass of the birds performing flights which were analysed was 43.6±1.2 g (mean ± S.E.M., N=6). This was not significantly different (P=0.3) from the mass of the birds used in the *in vitro* assessment of the mechanical power output of the pectoralis (Askew and Marsh, 2001). All power outputs are expressed as W kg^{-1} of pectoralis muscle averaged over a complete wingbeat cycle.

Fig. 3. Distribution of area (A) and mass (B) along the wing, which was divided into 11 strips of equal width, normal to the wing axis (C).

Table 2. *Morphological data for blue-breasted quail*
Coturnix chinensis

Body mass (g)	43.6±1.2 (6)
Pectoralis mass (%M_b)	15.0±0.6 (10)
Wing length (cm)	9.6±0.1 (6)
Wing mass (g)	1.7±0.06 (6)
Wing span (cm)	22.0±0.3 (6)
Wing area (cm^2)	97.7±1.5 (6)
Wingbeat frequency (Hz)	23.2±0.4 (5)
Relative downstroke duration	0.70±0.01 (5)
Strain	0.234±0.014 (5)
Average flight speed (m s^{-1})	4.9±0.2 (6)
Average elevation, χ (degrees)	78.2±2.0 (6)
$\dot{z}$ (m s^{-1})	4.8±0.2 (6)

NB wing area is the area of both wings, including the area of the body between the wing bases.

Values are means ± S.E.M. (N).

M_b, body mass; $\dot{z}$, velocity of the centre of mass in the z direction.
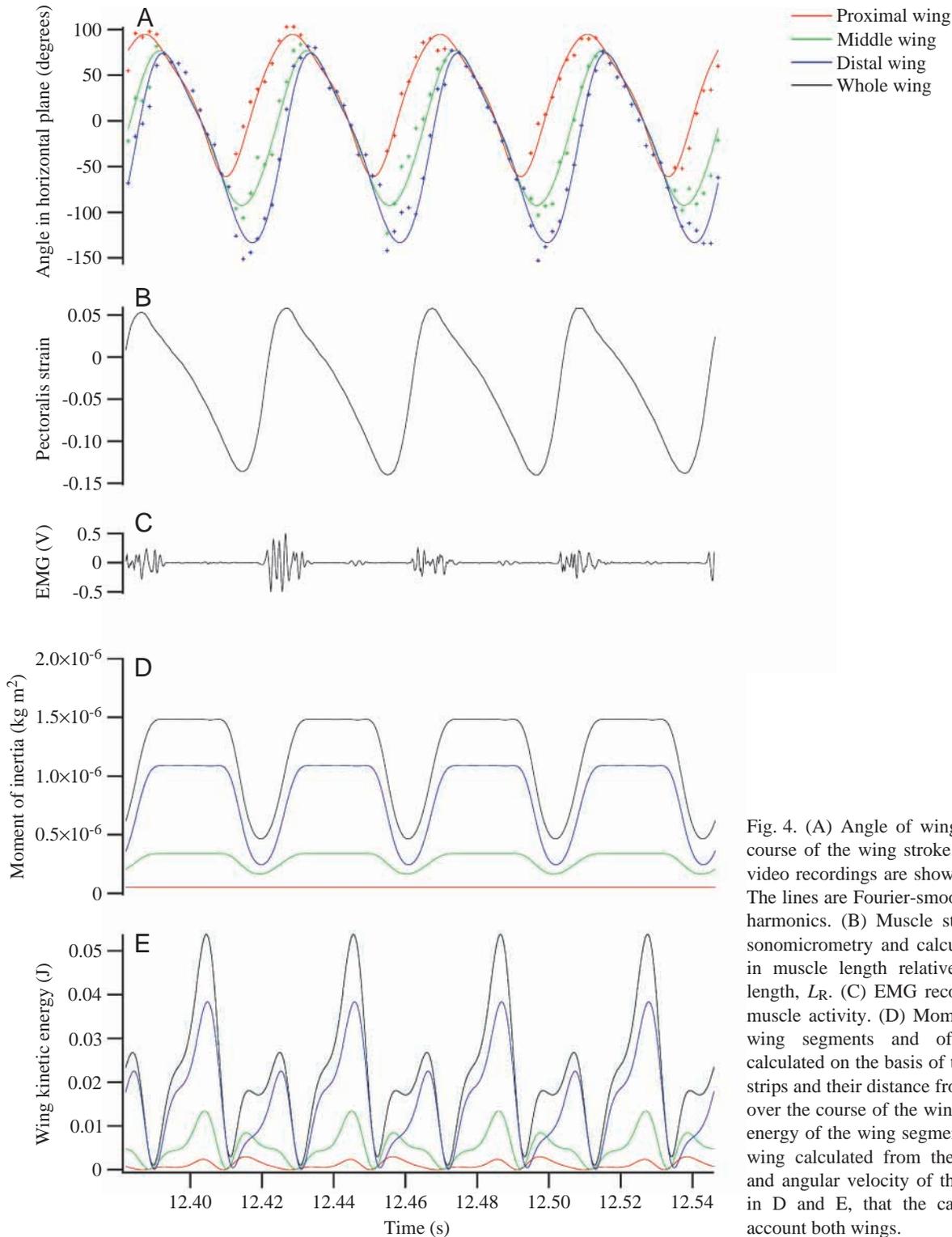
Fig. 4. (A) Angle of wing segments over the course of the wing stroke. Raw data from the video recordings are shown by the + symbols. The lines are Fourier-smoothed data with three harmonics. (B) Muscle strain recorded using sonomicrometry and calculated as the change in muscle length relative to resting muscle length, L_R. (C) EMG recordings of pectoralis muscle activity. (D) Moment of inertia of the wing segments and of the whole wing calculated on the basis of the mass of the wing strips and their distance from the shoulder joint over the course of the wing stroke. (E) Kinetic energy of the wing segments and of the whole wing calculated from the moment of inertia and angular velocity of the wing strips. Note, in D and E, that the calculations take into account both wings.

Wing mass and area distribution

Fig. 3 shows the distribution of mass and area in 11 equal-width strips perpendicular to the wing axis. Most of the mass of the wing was located close to the wing base. The proximal, middle and distal wing segments represented 46, 33 and 21 % of the total wing mass, respectively. The wing strips with the greatest area were those in the middle wing segment and at the base of the distal wing segment (each strip from these regions was 12–13 % of the total wing area). The distal wing had the largest area of the three wing segments, representing 62 % of the total area of the wing.

Wing position and correlation with pectoralis strain

Fig. 4 shows the change in the angle of the proximal, middle

A

Dorsal 6.5

Upstroke

4.3

2.2

0

43.1

40.9

38.8

36.6

34.5

32.3 Ventral

B

8.6 10.8

12.9

15.1

17.2

19.4

Downstroke

Shoulder

21.6

Elbow

Wrist

23.7

25.9

Wing tip 28.0

30.2

C

Wing tip

Wrist

Elbow

Shoulder
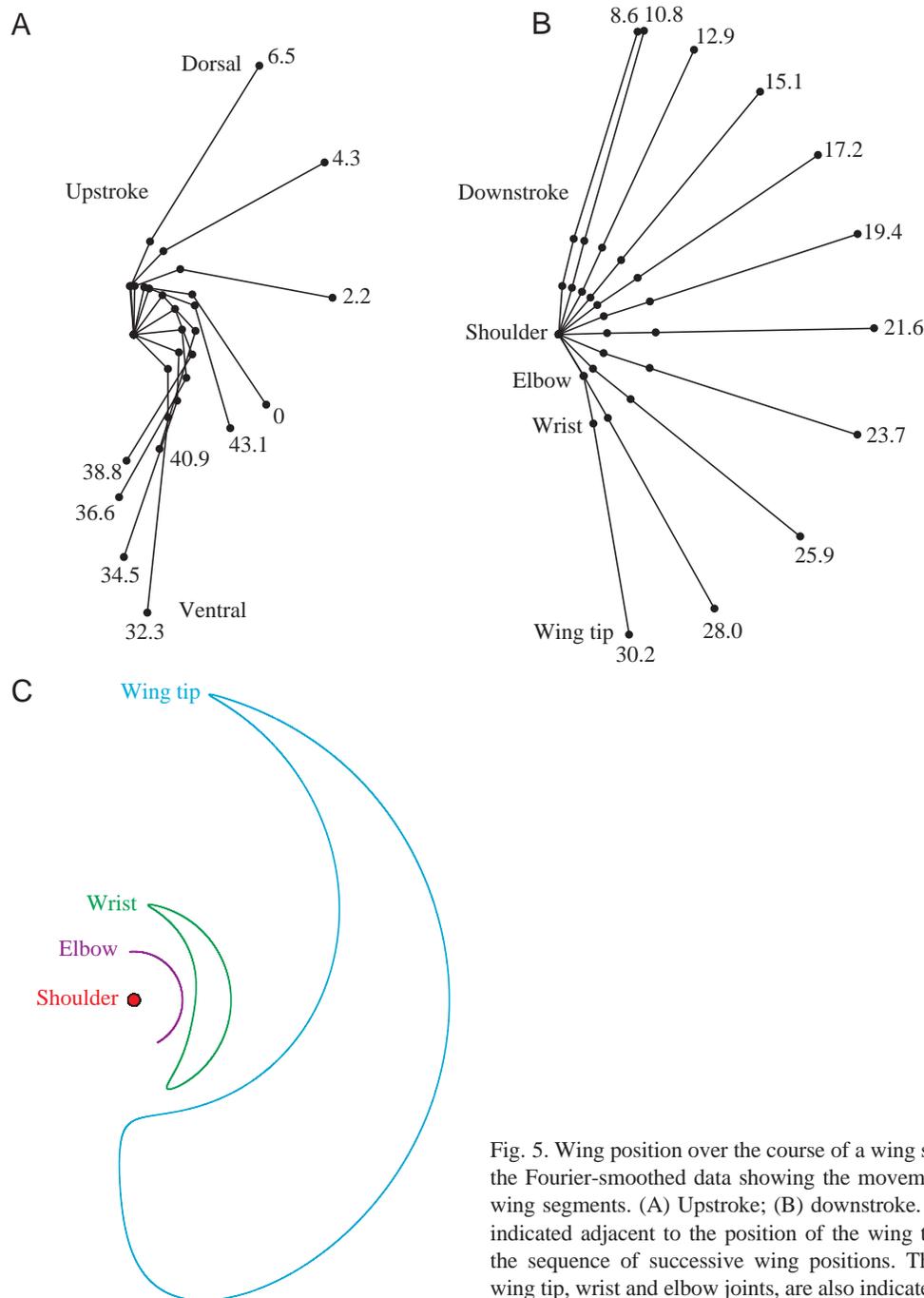
Fig. 5. Wing position over the course of a wing stroke calculated from the Fourier-smoothed data showing the movements of the individual wing segments. (A) Upstroke; (B) downstroke. Relative time (ms) is indicated adjacent to the position of the wing tip and serves to give the sequence of successive wing positions. The movements of the wing tip, wrist and elbow joints, are also indicated (C).

and distal wing segments in the horizontal plane over four wing strokes. There was some uncertainty about the position of the proximal wing in its most depressed position because it became obscured by the body. The proximal wing reaches its maximum elevation earliest in the wing stroke, followed by the middle wing (4.2 ms later) and the distal wing (a further 0.9 ms later). The proximal wing reaches a higher maximum angle of elevation (95°) compared with the other wing segments (both approximately 75°). Over the entire wing stroke, the total angle of excursion of the wing segments increases from wing base to tip (Table 3).

Fig. 5 shows the position of the wing over the course of a wing stroke, described by the Fourier-smoothed data. The positions of the wing tip, wrist, elbow and shoulder joint are also shown. The highest angle of elevation is attained by the proximal wing at the end of the upstroke. As the proximal wing starts to move downwards, it becomes aligned with the middle and distal wing segments after 4 and 5 ms, respectively. The wing remains aligned until late in the downstroke. The middle and distal wing segments continue to be depressed after the proximal wing starts to be elevated, with the distal wing movements also lagging behind those of the middle wing. The

Table 3. *Characteristics of the movements of the three wing segments for one quail during a vertical take-off flight*

Angle	Relative time for maximum angle of elevation (ms)	Maximum angle of excursion (degrees)
α	0	155.8
β	4.18	169.6
γ	5.04	207.4

α, β, γ are the angles between the horizontal plane and the proximal, middle and distal wing, respectively.

lag between the movements of the proximal wing and the middle wing, and between the middle wing and the distal wing, results in folding of the wing during the upstroke.

The strain of the pectoralis muscle, measured using sonomicrometry, showed an asymmetrical trajectory, shortening for approximately 70 % of the wing-stroke duration. The rate of shortening was not constant, with two periods of acceleration during shortening. The muscle's shortening velocity was highest at the end of the shortening period. The maximum muscle length (L_{max}) occurs 1.1 ms before the maximum angle of elevation of the proximal wing (Fig. 4).

Power output based on the movement of the centre of mass

To be fully analysed, a flight had to show predominant displacement in the *z*-axis (e.g. Fig. 2). In all, six flights were suitable for analysis, with an average elevation of almost 80° (Table 2). Fig. 2 shows a two-dimensional (Fig. 2A) and a three-dimensional (Fig. 2B) representation of a typical quail take-off flight. The scales of the axes in Fig. 2B have been selected so that they represent the actual dimensions of the flight chamber. Also shown are the quadratic equations and regression coefficients for the change in each dimension with time for this particular flight. On the basis of the overall acceleration and velocity of the centre of mass of the quail, the mean rate of change of kinetic energy was $-1.8 \pm 41.8 \, \text{W kg}^{-1}$ (mean ± S.E.M., $N=6$). The power required to increase the potential energy of the centre of mass was $314.6 \pm 10.4 \, \text{W kg}^{-1}$ (mean ± S.E.M., $N=6$) (Table 4).

Induced power output

The total area swept by the wings was $3.65 \times 10^{-2} \, \text{m}^2$, based on the wing movements illustrated in Fig. 4A. For the flights analyzed, the mean vertical velocity was $4.81 \, \text{m s}^{-1}$. The induced velocity for take-off at the mean upward acceleration of $-0.86 \, \text{m s}^{-2}$ was $0.78 \, \text{m s}^{-1}$ (equation 11). The induced power output required to generate the induced velocity *per se*, P_{ind}', was $61.3 \, \text{W kg}^{-1}$ assuming zero vertical acceleration of the bird. The average vertical acceleration for the flights analyzed was $-0.86 \, \text{m s}^{-2}$ (i.e. a deceleration), giving a P_{ind}' of $55.9 \, \text{W kg}^{-1}$, and the highest vertical acceleration measured was $2.16 \, \text{m s}^{-2}$, giving a P_{ind}' of $74.8 \, \text{W kg}^{-1}$ (Table 4).

Table 4. *Estimates of the muscle-mass-specific climbing, aerodynamic and inertial power requirements during take-off flights in blue-breasted quail* Coturnix chinensis

	Power output (W kg^{-1})	
	Mean for all flights	Maximum
Climbing power		
$dE_{K,ext}/dt$	-1.8 ± 41.8 (6)	135.2
dE_P/dt	314.6 ± 10.4 (6)	299.4
Induced power, P_{ind}'	55.9	74.8
Profile power, P_{pro}	18.8	20.1
Parasite power, P_{par}	2.0	1.8
Total aerodynamic power, P_{aero}		
$P_{aero} = \dfrac{dE_{K,ext}}{dt} + \dfrac{dE_P}{dt} + P_{ind}' + P_{pro} + P_{par}$	389.5	531.2

The calculation of profile power assumes that the angle of the stroke plane with respect to the horizontal is 0°.

The maximum values are the highest recorded for an individual quail (flight illustrated in Fig. 2).

$E_{K,ext}$, kinetic energy of the centre of mass; E_P, potential energy of the centre of mass; *t*, time.

Parasite power

The parasite power was $2.0 \, \text{W kg}^{-1}$ using a $C_{D,par}$ of 0.13. In relation to all the other powers that must be supplied by the pectoralis muscle during these take-off flights, the parasite power is negligible.

Profile power

The profile power output was calculated from the drag acting upon the wing (equation 15). Profile power was dependent on the angle of the stroke plane relative to the horizontal (φ). The mean downstroke profile power averaged over the entire wing stroke ranged between $8.0 \, \text{W kg}^{-1}$ (φ=30°; $w=0.785 \, \text{m s}^{-1}$; $\ddot{z}=-0.86 \, \text{m s}^{-2}$) and $19.7 \, \text{W kg}^{-1}$ (φ=0°; $w=1.007 \, \text{m s}^{-1}$; $\ddot{z}=2.16 \, \text{m s}^{-2}$), however we assumed a value of $18.8 \, \text{W kg}^{-1}$ (Table 4; φ=0°; $w=0.781 \, \text{m s}^{-1}$; $\ddot{z}=-0.86 \, \text{m s}^{-2}$) in subsequent calculations.

Total aerodynamic power output

The total aerodynamic power requirement, P_{aero}, of the pectoralis muscle was calculated as:

$$P_{aero} = \frac{dE_{K,ext}}{dt} + \frac{dE_P}{dt} + P_{ind}' + P_{pro} + P_{par} \qquad (21)$$

and was equal to $390 \, \text{W kg}^{-1}$ (Table 4).

Inertial power output

The moment of inertia of the whole wing (Fig. 4D) was maximal during the downstroke and equaled $1.48 \times 10^{-6} \, \text{kg m}^2$. This is slightly larger than the value predicted from the regression equation given by van den Berg and Rayner [$1.35 \times 10^{-6} \, \text{kg m}^2$ (van den Berg and Rayner, 1995)]; however,

in our calculations, we included the virtual mass. During the upstroke, the wing's moment of inertia was reduced to approximately one-third ($4.64\times10^{-7}\,\mathrm{kg\,m^2}$) of the maximum during the downstroke as a result of flexion of the wing.

Fig. 4E shows the fluctuation in the kinetic energy of each wing segment and of the whole wing over the course of the wing stroke. The total kinetic energy of the wing was dominated by the kinetic energy of the distal wing. The maximum kinetic energy of both wings was 0.054 J during the downstroke and 0.027 J during the upstroke. The kinetic energy of the distal wing represented 71 % of the total maximum kinetic energy of the wing during the downstroke. The large amount of kinetic energy in the distal wing resulted primarily from its large moment of inertia (Fig. 4D). The segments towards the tip of the wing were very light (Fig. 3), and the majority of the kinetic energy of the distal wing (49 %) was due to the movements of the two segments nearest to the wrist joint. The middle wing contributed 25 % of the maximum kinetic energy of the wing during the downstroke. Wing flexion during the upstroke reduced the maximum kinetic energy of the wing by half. The kinetic energy of the wing at the start of the upstroke was largely due to the movements of the proximal and middle wing segments, with the distal wing contributing most of the kinetic energy towards the end of the stroke.

During the first half of the downstroke, the pectoralis muscles must do 0.054 J of work to impart kinetic energy to the wings. This energy can then be used to perform aerodynamic work during the second half of the downstroke. However, if the kinetic energy is greater than the aerodynamic requirement, the excess energy would have to be dissipated or stored elastically. The aerodynamic power of the pectoralis is $390\,\mathrm{W\,kg^{-1}}$ when averaged over a cycle (Table 4). Given a pectoralis muscle mass of 6.54 g and a wingbeat frequency of 23.2 Hz (Table 1), the aerodynamic work during the downstroke is $390\times0.00654\times(1/23.2)=0.110\,\mathrm{J}$. Half of this work, i.e. 0.055 J, is done while the wings are accelerating during the first half of the downstroke, and this is greater than the kinetic energy of 0.054 J imparted to the wings. The other half of the aerodynamic work is done while the wings are decelerating, and the transfer of kinetic energy to work would reduce the contribution of the pectoralis to only $0.055-0.054=0.001\,\mathrm{J}$ during the second half of the downstroke. Thus, there is no need to postulate dissipation or elastic storage of the kinetic energy of the flapping wings; it can all be used for aerodynamic work. The inertial power requirement is therefore zero: power expended on accelerating the wings is recovered as aerodynamic power later in the downstroke.

Discussion

Wing movements and correlation with muscle strain

The proximal and distal wings were aligned throughout the majority of the downstroke (Fig. 4, Fig. 5). However, the movements of the middle and distal wing lagged behind those of the proximal wing. Thus, the middle and distal wing continued to be elevated after the proximal wing started to be depressed. At the end of the downstroke, the middle and distal wings continue to move downwards after the proximal wing started to be elevated. The result is that the wing is relatively flexed during the upstroke. This flexion serves two main functions. First, the inertial torque about the shoulder joint is reduced on the upstroke, because the wing mass is closer to the shoulder joint (Fig. 5). Second, it reduces the lift during the upstroke, which is important for net positive thrust over the entire wing stroke (Rayner, 1993). The lag between the movements of the proximal, middle and distal wing makes it difficult to define the start and end of the downstroke and upstroke on the basis of wing kinematics. Similar wing kinematics have been observed in other birds, for example, in the Andean condor [see fig. 1 in McGahan (McGahan, 1973)] and other species in the Phasianidae [see fig. 8 in Tobalske and Dial (Tobalske and Dial, 2000)].

The strain of the pectoralis muscle followed a very similar time course to the angle of the proximal wing (Fig. 4A,B). This similarity in time course undoubtedly results from the insertion of the pectoralis muscle onto the deltopectoral crest of the humerus. However, our measurements appear to indicate that the proximal wing started to be elevated before re-lengthening of the pectoralis muscle. This discrepancy is probably associated with the difficulty in measuring the angle of the proximal wing at the end of the downstroke, when it was often obscured by the body. At the end of the upstroke, shortening in the pectoralis fibres began 1.1 ms before the proximal wing started to move downwards. In the absence of angular movement, the initial fibre shortening could be due to the pectoralis lengthening of series elastic structures or causing an initial rotation of the humerus before depression of this element begins.

Early in the downstroke, the shortening velocity of the pectoralis muscle is quite high and then rapidly decreases to a brief minimum before increasing again (Askew and Marsh, 2001) (Fig. 4B). The initial rapid deceleration occurs at approximately the same time that the wing segments extend and become aligned ($\alpha=\beta=\gamma$). We suggest that the decrease in the muscle's shortening velocity coincides with an increase in the load on the wing due to the unfurling of the folded wing and the resulting increase in aerodynamic load. The velocity of shortening decreases as a result of the inverse relationship between force and velocity that is a property of all muscles, i.e. the force/velocity effect. This interaction between the pectoralis and the wing illustrates the subtle interplay between physiology and morphology that characterizes animal movement. The initial shortening of the pectoralis probably contributes to the unfurling of the wing (Garrod, 1875; Fisher, 1957; Dial, 1992), and the change in the wing shape then feeds back to alter the strain trajectory of the muscle.

Subsequent to the initial decrease in the velocity of shortening of the pectoralis during the downstroke, the rate of shortening of the muscle increased continuously almost to the end of the depression of the proximal wing. Rapid shortening facilitates muscle deactivation (Askew and Marsh, 1998), which could be important in minimizing the work required to

re-lengthen the muscle during the upstroke. It has been suggested that the acceleration of shortening, coupled with the distinctly asymmetrical cycles found in quail (and other species of bird), plays a major role in enhancing power output during flight (Askew and Marsh, 2001). This deactivation of the muscle fits in with the reduction in the work required of the pectoralis muscle during the latter half of shortening by using the kinetic energy of the wing to do aerodynamic work. In addition, feedback of the reduced power requirements is consistent with the increase in the rate of shortening (force/velocity effects).

Comparison of the strain trajectory in different bird species

Sonomicrometry measurements on the pectoralis muscle of several different bird species are now available: blue-breasted quail (Askew and Marsh, 2001), northern bobwhite, chukar, ring-necked pheasant, turkey (Tobalske and Dial, 2000), mallard (Williamson et al., 2001) and pigeon (Biewener et al., 1998). The strain trajectory for the turkey pectoralis is approximately sinusoidal; however, in all other species, the strain trajectory is distinctly asymmetrical, with muscle shortening occupying a greater proportion of the cycle than lengthening. In all these species, except for the turkey, the shortening velocity is low at the start of shortening and then increases towards the end of shortening [see fig. 6 in Tobalske and Dial (Tobalske and Dial, 2000)]. *In vitro* experiments using the pectoralis muscle from blue-breasted quail compared this type of shortening pattern with sawtooth cycles with the same relative proportion of shortening (Askew and Marsh, 2001). It was found that the *in vivo* length trajectory enhanced the power output by approximately 16% compared with the cycles with a constant shortening velocity. A higher peak lengthening velocity resulted in greater activation and led to higher instantaneous power outputs towards the end of shortening, compared with the sawtooth cycles.

Power requirements and power available

The total power output required over the course of a wing stroke for vertical take-off flight in blue-breasted quail was an impressive $390\,W\,kg^{-1}$ of pectoralis muscle mass. Although this value seems very high compared with many other estimates of muscle power output, it seems very unlikely to be in substantial error. Most of the power required was used to increase the potential energy of the centre of mass ($dE_P/dt=81\%$ of P_{aero}). This component of the power is not dependent on aerodynamic theory and cannot be disputed. Despite any vagaries of aerodynamic calculations, our estimate of $390\,W\,kg^{-1}$ seems realistic given the addition of induced power and the rate of increase of the kinetic energy of the body. The power required to accelerate the wings at the start of the downstroke was comparable with, but slightly less than, the aerodynamic power requirement, and we assume that it can be recovered for the aerodynamic requirements in the second half of the downstroke (Dudley and DeVries, 1990).

In a companion study (Askew and Marsh, 2001), the power available from the pectoralis muscles of blue-breasted quail was also determined *in vitro* by subjecting isolated bundles of fibres to the strain and activity patterns measured *in vivo* using the work loop technique (Askew and Marsh, 2001). Force was measured over the course of the simulated cycle and, hence, the power output was determined. The mean power output of the quail pectoralis muscle *in vitro* during the shortening phase of simulated flight strain trajectories was approximately $350\,W\,kg^{-1}$ averaged over the entire wing stroke. This value measured only during shortening is the appropriate one to compare with the values obtained here from kinematic measurements. Any work done on the pectoralis to lengthen it will not be detected in the mechanical power measured during flight. However, the work required to re-lengthen the muscle will contribute to the overall metabolic cost of flight, which we do not consider in this study. This is 90% of that calculated to be required on the basis of the movement of the centre of mass of the quail and the aerodynamic power. However, the highest power output measured *in vitro* was $433\,W\,kg^{-1}$ (Askew and Marsh, 2001), which is 18% lower than the highest power for an individual quail flight ($531\,W\,kg^{-1}$; Table 4).

Comparison with other in vivo power estimates

The power output calculated to be required from the pectoralis muscle of blue-breasted quail and the comparable estimates from *in vitro* preparations are very high in comparison with *in vivo* and *in vitro* estimates of power output in cyclically contracting muscles from animals other than birds. For example, the adductor muscle of swimming scallops generates $30\,W\,kg^{-1}$ (Marsh and Olson, 1994), the external oblique calling muscles of hylid tree frogs generate $50–60\,W\,kg^{-1}$ (Girgenrath and Marsh, 1999) and the white muscle of fish during fast starts produces $143\,W\,kg^{-1}$ (Wakeling and Johnston, 1998). It should be noted that these power outputs are obtained at relatively lower temperatures ($10–25\,°C$) than the body temperature of birds (approximately $40\,°C$). In insects with synchronous flight muscle (the insects' equivalent of vertebrate striated muscle), the power output estimated to be required from the flight muscles of hawkmoths is $90–150\,W\,kg^{-1}$ [determined from *in vitro* work loop experiments at $40\,°C$ (Stevenson and Josephson, 1990); estimated using aerodynamic theory (Willmott and Ellington, 1997)] and in dragonflies, $160\,W\,kg^{-1}$ [estimated using aerodynamic theory (Wakeling and Ellington, 1997b)].

In birds, the power output required from the pectoralis muscle has been estimated recently from *in vivo* force measurements using strain gauges attached to the deltopectoral crest (DPC) of the humerus, coupled with estimates of muscle strain based either on wing kinematics or on sonomicrometry measurements. Using these techniques, the following power outputs have been reported (see also Fig. 6): $51–70\,W\,kg^{-1}$ [pigeon level flight (Dial and Biewener, 1993; Biewener et al., 1998)], $119\,W\,kg^{-1}$ [pigeon take-off (Dial and Biewener, 1993)], $104\,W\,kg^{-1}$ [starling level flight (Biewener et al., 1992)], $60\,W\,kg^{-1}$ (magpie level flight), $143\,W\,kg^{-1}$ [magpie hovering flight (Dial et al., 1997)], $130\,W\,kg^{-1}$ (mallard level flight) and $175\,W\,kg^{-1}$ [mallard ascending flight (Williamson et al., 2001)]. These measurements,
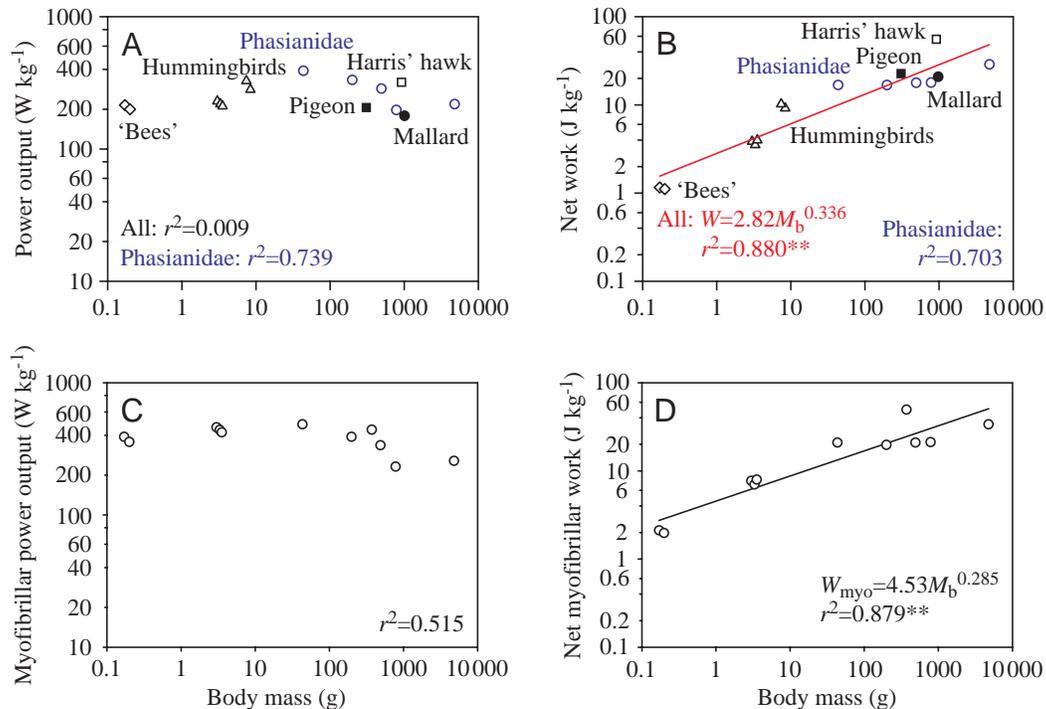
Fig. 6. Scaling of (A) pectoralis muscle power output and (B) net work per wing stroke with body mass M_b. Data are shown for the Phasianidae (open circles), pigeon and Harris' hawk during take-off (from Table 5), for hummingbirds (Chai and Millard, 1997; Chai et al., 1997), 'bees' (euglossine bees, *Euglossa imperialis*; M. E. Dillon and R. Dudley, in preparation) and worker bumblebees (Cooper, 1993) during loaded hovering or loaded climbing flights. Scaling of (C) pectoralis myofibrillar power output and (D) net myofibrillar work per wing stroke (W_{myo}) with body mass. In C and D, data are shown for the Phasianidae, pigeon, small hummingbirds and 'bees', calculated by assuming relative myofibrillar volumes of 0.85 (Kaiser and George, 1973; Kiessling, 1977), 0.47 (George and Berger, 1966), 0.50 (Suarez et al., 1991) and 0.55 (Casey and Ellington, 1989), respectively. Relationships that are significantly different from zero are denoted by *($P<0.05$) and **($P<0.01$).

based as they are on *in vivo* measures of force and length change, represent the most direct measurements of power output of the pectoralis during flight. However, they are considerably lower than the values we have calculated here and measured *in vitro* for the pectoralis of blue-breasted quail and are also lower than values calculated for other species in the family Phasianidae and for a species of hawk during climbing flights shortly after take-off (Fig. 6; Table 5) (Askew and Marsh, 2001).

Why does this apparent discrepancy exist between our power estimates and the more direct estimates based on *in vivo* stress and strain recordings (DPC technique)? First, it should be pointed out that power output in level flight is expected to be lower than that during the rapid vertical flights we studied. However, two of the estimates using the DPC technique were made during climbing and one during hovering, which are activities requiring a high power output, and these estimates are still considerably below the 350–530 W kg^{-1} that we have calculated here and measured *in vitro* (Askew and Marsh, 2001). Dial and Biewener (Dial and Biewener, 1993; Biewener et al., 1998) have suggested that some estimates based on aerodynamic estimates may be too high because of unsteady lift-generating mechanisms. However, unsteady lift-generating mechanisms do not decrease the power required to generate lift. Instead, unsteady mechanisms should be understood as a way of increasing the lift that can be generated. Power must

still be expended to generate this extra lift. Unsteady mechanisms would affect the profile power estimate, but the profile power is only 5 % of the total aerodynamic power requirement in the blue-breasted quail. Errors may exist in the DPC techniques used *in vivo*, either in the measures of muscle stress or in the muscle strain estimated by kinematic techniques. The potential difficulties in calibrating the strain gauges on the DPC have been carefully considered by the authors (Dial and Biewener, 1993; Williamson et al., 2001).

Assessing the level of disagreement between our results and the DPC-based measurements first requires an estimate of the aerodynamic power required in the species studied using this technique. The most useful comparison for our purposes involve the data on climbing flights in pigeons. Sufficient data exist to calculate the power requirements during the climbing flights measured by Dial and Biewener (Dial and Biewener, 1993). The birds required 129 W kg^{-1} to raise their centre of mass (dE_P/dt) at the reported rate of 2.62 m s^{-1}. During climbing, however, the birds also have substantial induced power requirements. The induced power term will be lower than that for hovering flight as the result of an increased air flow through the actuator disc from the vertical climbing speed (Cooper, 1993). Thus, the importance of this term varies with the rate of climbing. In blue-breasted quail, which take-off at a high velocity, P_{ind}' is quite low, but for some of the larger

species in the Phasianidae the low rates of climb result in P_{ind}' being the dominant power component. We have calculated the total power requirements for pigeons during the climbing flights measured by Dial and Biewner (Dial and Biewner, 1993) using data from Pennycuick and Parker (Pennycuick and Parker, 1966), Pennycuick (Pennycuick, 1968) and Dial and Biewener (Dial and Biewener, 1993). The total aerodyamic power is approximately $206\,W\,kg^{-1}$ (Table 5; Fig. 6A). This value is 1.7 times the $119\,W\,kg^{-1}$ estimated by Dial and Biewener (Dial and Biewener, 1993) using measurements of force on the DPC and muscle length change based on wing kinematics.

More recently, Biewener et al. (Biewener et al., 1998) report improved measurements of *in vivo* work loops in pigeons using sonomicrometry to estimate the changes in muscle length. This newer study does not report values during climbing, but during level flight the net power output is reported to have a mean of $70\,W\,kg^{-1}$, a 37 % increase over the estimates of Dial and Biewener (Dial and Biewener, 1993). However, the actual power outputs in the newer study are even higher. Biewener et al. (Biewener et al., 1998) arrived at the estimate of $70\,W\,kg^{-1}$ by correcting downwards their raw values of approximately $90\,W\,kg^{-1}$. This correction was based the mean fascicle length in the muscle being shorter than the length of the fascicles at the sonomicrometer site. However, correction for mean fibre length is not necessary; the relevant length change for calculating the power output is the length change along the axis of the central tendon because this is where the measured force is being exerted. This length change can be estimated from the length change in any group of fascicles as long as the fibre angle is known (A. A. Biewener, personal communication). Shorter fascicles either insert at higher angles and thus maintain similar strain for the same length change in the tendon (Gans and Gaunt, 1991) or they must have higher strains. The value of $90\,W\,kg^{-1}$ for net power output may still be a slight underestimate after taking into consideration the fibre angle.

To compare this net power with any calculations based on aerodynamic power further requires adding back the negative power measured during the upstroke to arrive at the power produced during the downstroke. As we have pointed out here, the internal power loss during the upstroke does not show up in the transfer of power to the environment. Biewener et al. (Biewener et al., 1998) report that the negative power is 15 % of the total power, and thus we arrive at an estimate of positive power of $106\,W\,kg^{-1}$. This new estimate during level flight is approximately twice the original estimate of Dial and Biewener (Dial and Biewener, 1993). If the original estimates of power during climbing were also too low by a similar factor, then the apparent discrepancy between aerodynamic power and the power measured by the DPC technique would disappear. These same problems with calculating DPC power apply to the other published values (A. A. Biewener, personal communication), but not all the necessary data are available in the publications to correct the values cited above.

If this assessment of the DPC technique is correct, then the real question becomes why do pigeons during climbing produce so much less power than the other birds for which we report data (P_{aero}; Table 5)? Several explanations for the lower power outputs in pigeons are possible. First, the low wingbeat frequencies (approximately 9 Hz) used by pigeons may limit power output. However, calculations of climbing power in Harris' hawks and turkeys (Table 5; Fig. 6, see also section on scaling below) result in higher power outputs than the value for pigeons despite similar wingbeat frequencies. Second, the differences in power output could result from differing fibre types and/or their recruitment. Pigeons are well known for having two very distinct fibre types in their flight muscles. Approximately 14 % of the fibres are large ($70\,\mu m$ in diameter) low-oxidative fibres, and the remaining 86 % are much smaller ($30\,\mu m$ in diameter) high-oxidative fibres (George and Berger, 1966). Thus, roughly equal volumes of the muscle are occupied by high- and low-oxidative fibres. This contrasts with the burst flying phasianids, which are likely to have most of the fibre volume occupied by low-oxidative fibres (Kaiser and George, 1973; Kiessling, 1977).

The oxidative fibres in pigeons might be expected to have a large volume of mitochondria and lipid droplets, thus commensurately reducing the power output per fibre volume. However, the density of mitochondria and lipid droplets (20 % and 4 % of fibre volume, respectively) found in pigeon high-oxidative fibres (Mathieu-Costello et al., 1998) coupled with the percentage of muscle volume occupied by high-oxidative fibres does not seem large enough to account for the lower power output found in these animals. However, differential recruitment of these fibre types could reduce power output during climbing. The possibility exists that the two fibre types represent a 'two-geared' system in which only the low-oxidative fibres are recruited for high-power activities such as take-off and rapid climbing, and the high-oxidative fibres are recruited exclusively in more sustained activities. This alone would fully account for the twofold difference in power output between the pectoralis muscles of pigeons and blue-breasted quails. Third, the explanation could be very much simpler. The recorded climbing rates in pigeons may underestimate the maximal performance of these birds.

Scaling of power, work, strain and stress in the pectoralis muscle

An understanding of how the maximum power available from the flight muscles scales with body size is important in determining the limits of flight performance, such as the maximum size of bird that can fly, and in determining how much excess power is available for climbing flight (Pennycuick, 1975). Various estimates have been made of the scaling of power output with body mass. Pennycuick (Pennycuick, 1975) predicted that the maximum power available from the flight muscles should scale as $M_b^{-1/3}$. This was based on the assumption that stress, strain and, therefore, work should be independent of body size. Under these assumptions, the maximum power available will scale with maximum wingbeat frequency, which is predicted to scale as $M_b^{-1/3}$. Ellington (Ellington, 1991) reported that the muscle-

Table 5. *Aerodynamic power components during take-off flight*

	Harris' hawk	Pigeon	Blue-breasted quail	Northern bobwhite	Chukar	Ring-necked pheasant	Turkey
Body mass, M_b (g)	920[a]	307[b]	43.6	199.5[c]	491.5[c]	783.0[c]	4780.0[c]
Relative pectoralis muscle mass	0.140[d]	0.200[b]	0.150[e]	0.173[c]	0.145[c]	0.169[c]	0.156[c]
Wing length (cm)	52.2[f]	33.0[g]	–	13.8[c]	23.0[c]	30.6[c]	53.6[c]
Wing area (cm^2)	1190[h]	351.6[g]	94.2	242.8[c]	483.2[c]	1001.5[c]	3453.1[c]
Disc area, D (cm^2)	7085[i]	2700.7[j]	365.5[i]	466.4	1390.0[i]	2467.7[i]	8003.5[i]
Body frontal area, S_b (cm^2)[k]	76.9	37.0	13.9	27.8	50.7	78.2	246.1
Wingstroke amplitude (degrees)	149.0[l]	142.1[j]	–	140.3[c]	151.2[c]	151.0[c]	159.9[c]
Stroke plane angle (degrees)	57[m]	–	–	70[k]	80[k]	45[k]	50[k]
$-\alpha'$[n]	109.1	90	90	109.1	110.8	76.1	108.8
Wingbeat frequency (Hz)	5.8[a]	9.1[b]	23.2[e]	19.9[c]	16.1[c]	11.0[c]	7.6[c]
Vertical velocity (m s^{-1})	3.25[a]	2.62[b]	4.81[e]	2.05[o]	1.47[o]	1.12[o]	2.02[o]
Horizontal velocity (m s^{-1})	2.55	–	1.01	2.52[o]	2.46[o]	2.06[o]	1.15[o]
Horizontal acceleration (m s^{-2})	–	–	6.7	2.03[o]	2.19[o]	1.79[o]	3.74[o]
Vertical acceleration (m s^{-2})	–	–	–0.86	–0.23[o]	–1.59[o]	–1.14[o]	–3.88[o]
Induced velocity, w (m s^{-1})	1.04[q]	1.21[p]	0.78[p]	2.84[q]	2.37[q]	2.42[q]	2.88[q]
Resultant air velocity, V_R (m s^{-1})[r]	6.9	8.8	9.2	5.2	8.7	8.2	10.7
dE_P/dt[s] (W kg^{-1})	227.7	128.8	314.5	115.9	99.2	54.0	118.9
$dE_{K,ext}/dt$[t] (W kg^{-1})	–	–	20.2	26.8	21.0	14.4	–22.5
P_{ind}[u] (W kg^{-1})	87.1	71.5	55.9	188.2	159.9	123.8	114.8
P_{pro}[v] (W kg^{-1})	5.1	5.8	18.8	1.5	6.3	4.7	6.8
P_{par}[w] (W kg^{-1})	0.16	0.08	2.0	0.22	0.13	0.04	0.03
P_{aero}[x] (W kg^{-1})	320.0	206.2	411.3	332.7	286.5	196.9	218.0
W (J kg^{-1}) [y]	55.6	22.6	17.7	16.7	17.8	17.9	28.7

$-\alpha'$, the angle at which the velocity of the bird is inclined to the actuator disc (Wakeling and Ellington, 1997b); E_P, potential energy of the centre of mass; $E_{K,ext}$, kinetic energy of the centre of mass; t, time; P_{ind}', induced power required to generate the induced velocity; P_{pro}, profile power; P_{par}, parasite power; P_{aero}, total power; W, net pectoralis muscle work per wing stroke.

[a]Data taken from Pennycuick et al. (Pennycuick et al., 1989).

[b]Data taken from Dial and Biewener (Dial and Biewener, 1993).

[c]Data taken from Tobalske and Dial (Tobalske and Dial, 2000).

[d]Harris' hawk pectoralis muscle mass based on mean flight muscle mass in 17 species in the family Accipitridae (Hartman, 1961)

[e]Data from Askew and Marsh (Askew and Marsh, 2001).

[f]Harris' hawk wing length estimated to be $0.45 \times$ wing span (given by Pennycuick et al., 1989).

[g]Data from Pennycuick (Pennycuick, 1968).

[h]Harris' hawk wing area based on allometric analysis of wing area *versus* body mass in 17 species in the family Accipitridae (Hartman, 1961).

[i]Area of the actuator disc (D) calculated from the wing stroke amplitude×(wing length)^2.

[j]Data from Pennycuick and Parker (Pennycuick and Parker, 1966).

[k]Body area (S_b) calculated using the equation $S_b=0.00813M_b^{0.666}$ (Pennycuick et al., 1988), where M_b is body mass.

[l]Assumed amplitude based on the mean value for the other species in the table.

[m]Stroke plane angle estimated from a regression between take-off angle and stroke plane angle for Northern bobwhite, chukar and turkey.

[n]Inclination of the forward velocity of the bird to the actuator disc (as defined in Wakeling and Ellington, 1997b); bird velocity is assumed to be perpendicular to the actuator disc in pigeon and blue-breasted quail.

[o]Data from B. W. Tobalske (personal communication).

[p]Induced velocity (w) calculated using equation 11; bird velocity is assumed to be perpendicular to the actuator disc.

[q]Induced velocity (w) for an inclined flight path (calculated using equation 4 in Wakeling and Ellington, 1997).

[r]Resultant air velocity calculated from equation 16.

[s]Power required to increase the animal's potential energy (dE_P/dt) calculated using equation 10.

[t]Power required to increase the animal's kinetic energy ($dE_{K,ext}/dt$) calculated from $dE_K/dt=M_b\dot{z}\ddot{z}+M_b\dot{h}\ddot{h}$, where $\dot{h}$ is the velocity of the bird in the horizontal plane and $\ddot{h}$ is the acceleration of the bird in the horizontal plane. Note that this calculation of the rate of change of kinetic energy uses average velocities and accelerations and may include the contribution of power from the hindlimbs. $\dot{z}$ and $\ddot{z}$, velocity and acceleration, respectively, of the centre of mass in the z direction.

[u]Induced power (P_{ind}') calculated using equation 13.

[v]Profile power (P_{pro}) calculated using equation 15.

[w]Parasite power (P_{par}) calculated using equation 14 using a $C_{D,par}$ of 0.13.

[x]Aerodynamic power output (P_{aero}) calculated using equation 21.

[y]Work per wing stroke calculated as P_{aero}/wingbeat frequency.

mass-specific induced power output for a range of maximally loaded, flying animals (19 mg to 920 g) scaled as $M_b^{0.13}$. However, this positive scaling is based on calculations of maximum induced power output, which may not represent the same proportion of the total power required in different-sized animals. For example, whilst induced power will be the dominant power component in the larger species, it may represent only half the total power required in insects. Thus, the actual scaling exponent for available power may be lower than that indicated.

A recent study of four members of the family Phasianidae (Tobalske and Dial, 2000), all larger than the blue-breasted quail measured here, provides data that can be used to calculate power requirements during rapid take-off flights and to examine the influence of body size within this group.

Tobalske and Dial (Tobalske and Dial, 2000) reported the power required to move the bird's centre of mass, but the aerodynamic power requirements were not calculated. However, morphological and kinematic data in Tobalske and Dial (Tobalske and Dial, 2000) and some additional data provided by B. W. Tobalske (personal communication) enable us to calculate the total take-off power including the aerodynamic power requirements for these four additional species in the Phasianidae (equations 10, 13–15 and 21; see Table 5; Fig. 6). Our calculations for blue-breasted quail subtract out the initial kinetic energy of the body (see equation 9), which may include contributions from the hindlimbs. Unfortunately, we do not have sufficient data to enable us to eliminate the possible contribution from a hindlimb-powered jump in the four species from Tobalske and Dial's study (Tobalske and Dial, 2000). However, the mechanical power output of take-off power in jumping anurans is independent of mass (Marsh, 1994) and, if the same is true in the Phasianidae, the power provided by the hindlimbs during an initial jump will not affect the scaling of the power required from the pectoralis muscles.

Tobalske and Dial (Tobalske and Dial, 2000) report a high degree of variability in the flight behaviour in the pheasant family, with some individuals accelerating whilst others decelerated. This may be due to differences in the level of motivation and because their turkeys were trained to fly to a perch. As we are interested in maximal performance, we excluded from our calculations two individual birds (one pheasant and one turkey) which had much larger decelerations than other individuals within each species during take-off.

Across the species of phasianids that we examined, the mass of the pectoralis muscle scales in proportion with body mass ($r^2=0.998$, $P<0.002$; Fig. 7A), representing a constant 15 % of body mass. Therefore, the scaling of work and power per body mass is the same as the scaling per muscle mass.

Within the Phasianidae, there is no significant scaling of muscle-mass-specific power output with body mass; however, there is a tendency for power to decrease in the largest species ($\propto M_b^{-0.14}$; $r^2=0.739$; Fig. 6A). Take-off power ranged from approximately 200 W kg^{-1} (turkey and pheasant) to approximately 400 W kg^{-1} (blue-breasted quail) (Table 4),

with a mean value of 285 W kg^{-1} of pectoralis muscle across all species. Tobalske and Dial (Tobalske and Dial, 2000) found that the power required to move the centre of mass decreased with increasing mass, but the scaling relationship was steeper than that we have calculated [$\propto M_b^{-0.33}$ (Tobalske and Dial, 2000)]. Conclusions about the scaling of power output should, of course, be tempered by the caveat that it is assumed that the burst flight performance in these different-sized birds represents a similar percentage of the maximum effort possible.

In addition to our calculations for the Phasianidae, we have included data from similar calculations for vertical flights in the Harris' hawk and the pigeon (Table 5; Fig. 6A) (Pennycuick and Parker, 1966; Pennycuick, 1968; Dial and Biewener, 1993). As mentioned above, the values for pigeons are lower but, strikingly, the power output during climbing in the Harris' hawk is similar to that found in the phasianids, despite a much lower wingbeat frequency.

Maximal burst power output during load-lifting has also been estimated in hummingbirds, worker bumblebees and euglossine bees using similar methods to those that we have used here (Chai and Millard, 1997; Chai et al., 1997; Cooper, 1993) (M. E. Dillon and R. Dudley, in preparation). These animals have very high inertial power requirements because of their high wingbeat frequencies, and the calculations assume perfect elastic energy storage of the inertial power at the extremes of the wing strokes (Chai and Millard, 1997). Also, the calculated values assume that both the downstroke and upstroke flight muscles contribute equally on a mass-specific basis to the power for flight. The power outputs are somewhat over 200 W kg^{-1} of flight muscle for small 3–4 g hummingbirds and approximately 300 W kg^{-1} for larger 7–9 g birds. The maximal power outputs for *Euglossa imperialis* (170 mg euglossine bee) is approximately 215 W kg^{-1} (M. E. Dillon and R. Dudley, in preparation) and almost 200 W kg^{-1} for worker bumblebees [200 mg (Cooper, 1993)]. Thus, the power output in these species is somewhat lower than that required for take-off in the Phasianidae. However, the myofibrils in the smaller hummingbird species and euglossine bees typically represent only 50 or 55 %, respectively, of the flight muscle volume (Suarez et al., 1991; Casey and Ellington, 1989), the remainder being capillaries, sarcoplasmic reticulum and mitochondria. In these species, the myofibrillar power output ranges between 360 and 460 W kg^{-1} (Fig. 6C). If the phasianids studied, which have muscles consisting primarily of large low-oxidative fibres, have relative myofibrillar volumes of approximately 85 % [based on estimates for five members of the Phasianidae (Kaiser and George, 1973; Kiessling, 1977)], then the myofibrillar volume-specific power outputs would be similar, in all cases 230–460 W kg^{-1}. Regardless of the overall oxidative capacity of the muscles, the power outputs of the phasianids, hummingbirds, euglossine bees and the Harris' hawk are all short-term efforts that are not sustainable. Sustainable efforts, even in the highly aerobic hummingbirds and euglossine bees, result in considerably lower mechanical power outputs (Wells, 1993; Chai and Dudley, 1995; Casey
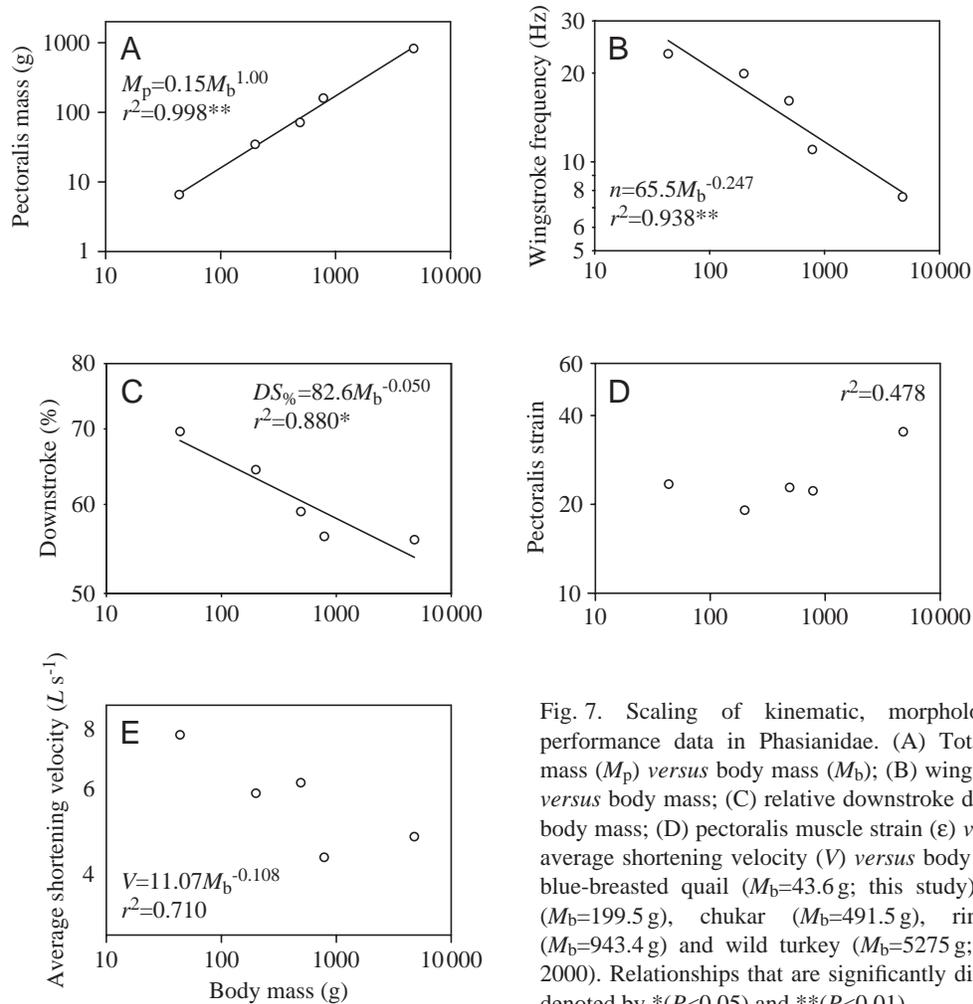
Fig. 7. Scaling of kinematic, morphological and muscle performance data in Phasianidae. (A) Total pectoralis muscle mass (M_p) *versus* body mass (M_b); (B) wing stroke frequency (n) *versus* body mass; (C) relative downstroke duration ($DS_\%$) *versus* body mass; (D) pectoralis muscle strain (ε) *versus* body mass; (E) average shortening velocity (V) *versus* body mass. Data are from blue-breasted quail (M_b=43.6 g; this study), northern bobwhite (M_b=199.5 g), chukar (M_b=491.5 g), ring-necked pheasant (M_b=943.4 g) and wild turkey (M_b=5275 g; Tobalske and Dial, 2000). Relationships that are significantly different from zero are denoted by *($P<0.05$) and **($P<0.01$).

and Ellington, 1989). The important conclusion we have reached on the basis of the data summarized here is that, over a size range of 170 mg to 4.78 kg, the burst myofibrillar power output of the flight muscles from insects and birds is remarkably high and is largely independent of mass (Fig. 6C; average myofibrillar power output 375 W kg^{-1}). This conclusion is all the more remarkable given that the animals encompass distinctly different flight styles and beat their wings with frequencies ranging from 5 to 186 Hz.

In the Phasianidae, wingbeat frequency decreases with increasing body mass, scaling as $M_b^{-0.247}$ (Fig. 7B; r^2=0.938, $P<0.01$). This allometry of wingbeat frequency and the tendency for power output to decrease with increasing mass means that the work per stroke is largely independent of body mass in the Phasianidae (17–18 J kg^{-1}), increasing only in the largest species (turkey 29 J kg^{-1}; Fig. 6B; r^2=0.703; not significant). Predicted work output in the turkey and Harris' hawk (29–56 J kg^{-1}) is very large, but these values are within the possible range for vertebrate muscle (Peplowski and Marsh, 1997). This level of work output has been found in muscles during jumping (Peplowski and Marsh, 1997), but has not been previously found to occur in repetitive contractions.

Including data for hummingbirds, Harris' hawk, mallard and two species of bees, gives a scaling of work per wing stroke as $M_b^{0.336}$ (r^2=0.880; $P<0.01$; Fig. 6B). Myofibrillar work per stroke also increases with increasing body mass, scaling as $M_b^{0.285}$ (r^2=0.879; $P<0.01$; Fig. 6D).

Muscle strain measured by sonomicrometry in the Phasianidae is approximately 22 % in birds ranging in size from 0.04 to 1 kg (Fig. 7D) (Tobalske and Dial, 2000) (this study). Measured strains are higher in the 5.3 kg turkey, but the overall scaling relationship is not significant (r^2=0.478). Because strain and work per stroke are relatively constant within the phasianids, the mean muscle stress is also independent of size and was approximately 85 kN m^{-2} in all species (Fig. 8).

The mean proportion of the wing stroke spent on the downstroke decreased significantly with increasing body mass ($P<0.05$), ranging from 70 % in blue-breasted quail to 56 % in ring-necked pheasant and wild turkey (Fig. 7C). However, as pointed out in the accompanying study (Askew and Marsh, 2001), all these species are capable of generating similar levels of asymmetry in the strain trajectory during some flights. The measured wingbeat frequency, relative downstroke duration
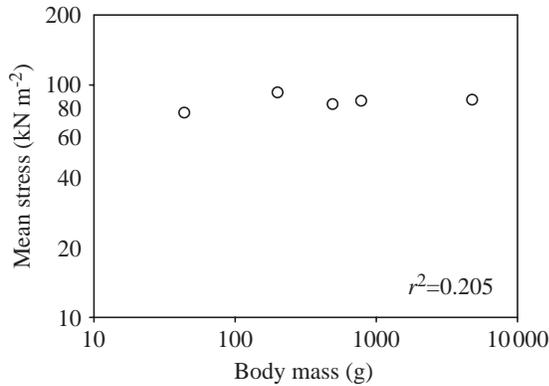
Fig. 8. Scaling of mean pectoralis muscle stress in the Phasianidae calculated from the mean take-off power, pectoralis muscle strain, muscle density and wingbeat frequency.

and muscle strain result in a scaling of the average muscle shortening velocity (V) as $M_b^{-0.108}$ ($P<0.1$; Fig. 7E). Data from fish, amphibian and mammalian muscles indicate that the maximum velocity of shortening scales with $M_b^{-0.07}$ to $M_b^{-0.13}$ (Rome et al., 1990; Seow and Ford, 1991; Marsh, 1994; James et al., 1998). If V_{max} scales with a similar exponent in the pectoralis muscle of the Phasianidae, then the length trajectory found in these birds enables all their pectoralis muscles to operate at a similar V/V_{max} (assuming that the curvature of the force/velocity relationship is the same in all species). If both the muscle strain and the relative downstroke duration *were* independent of body mass, the average shortening velocity would scale with wingbeat frequency ($\propto M_b^{-0.247}$). Manipulation of the strain trajectory might be one way of avoiding the unfavourable V/V_{max} that would result, whilst retaining the high wingbeat frequency required for aerodynamic reasons.

List of symbols

a, b	Fourier coefficients
A, B	distance between the optical centre of the lens of cameras 1 and 2, respectively, and the screen
c	mean chord of wing strip
$C_{D,par}$	parasite drag coefficient of the body
$C_{D,pro}$	profile drag coefficient of the wing
D	area of the actuator disc
$DS_\%$	relative downstroke duration
E	value predicted from a Fourier series
$E_{K,ext}$	kinetic energy of the centre of mass
$E_{K,int}$	kinetic energy of the wing
E_P	potential energy of the centre of mass
$\boldsymbol{g}$	gravitational acceleration
$\dot{h}$	average velocity of the centre of mass in the horizontal plane
$\ddot{h}$	average acceleration of the centre of mass in the horizontal plane
I	moment of inertia
k	induced velocity correction factor
L	muscle length
L_{max}	maximum muscle length
L_R	resting muscle length
m	mass of wing strip
m_v	virtual mass
M_b	body mass
M_p	pectoral muscle mass
n	harmonic number
N	number of data points
O	observed value
P_{aero}	total power
P_{ind}	induced power
P_{ind}'	the induced power required to generate the induced velocity *per se*
P_{par}	parasite power
P_{pro}	profile power
r	distance from a wing strip to the shoulder joint
Re	Reynolds number
S	wing strip area
S_b	frontal area of the body
t	time
v	velocity of the centre of mass
v_{mp}	minimum power speed
V	average shortening velocity
V_h	velocity of bird in the horizontal plane
V_{max}	maximum muscle shortening velocity
V_R	resultant velocity of the wing strip
w	induced velocity
W	net pectoralis muscle work per wing stroke
W_{myo}	net myofibrillar work
x, y, z	coordinates describing the three-dimensional position of the quail
$\dot{x}, \dot{y}, \dot{z}$	velocity of the centre of mass in the x, y and z directions, respectively
x_{im}, y_{im}, z_{im}	distance between the origin and the image of the bird in the x, y and z directions, respectively
$x_{max}, y_{max}, z_{max}$	dimensions of the field of view in the x, y and z directions, respectively
X	relative time ($-\pi$ to π)
$\ddot{z}$	vertical acceleration of the centre of mass
α, β, γ	angular position of the proximal, middle and distal segments, respectively, of the wing in the horizontal plane
$-\alpha'$	the angle at which the forward velocity of the bird is inclined to the actuator disc
$\alpha_f, \beta_f, \gamma_f$	Fourier-smoothed position of the proximal, middle and distal segments, respectively, of the wing in the horizontal plane
$\delta, \varepsilon, \phi$	opening angles of the camera
$\delta', \varepsilon', \phi'$	angles between the bird and the origin
χ	average angle of elevation of the flight with respect to the horizontal

φ   angle of the stroke plane with respect to the horizontal plane

ρ   air density

ω   angular velocity of a wing segment with respect to the shoulder joint

References

Askew, G. N. and Marsh, R. L. (1997). The effects of the length trajectory on the mechanical power output of mouse skeletal muscles. *J. Exp. Biol.* **200**, 3119–3131.

Askew, G. N. and Marsh, R. L. (1998). Optimal shortening velocity (V/V_{max}) of skeletal muscle during cyclical contractions: length–force effects and velocity-dependent activation and deactivation. *J. Exp. Biol.* **201**, 1527–1540.

Askew, G. N. and Marsh, R. L. (2001). The mechanical power output of the pectoralis muscle of blue-breasted quail (*Coturnix chinensis*): the *in vivo* length cycle and its implications for muscle performance. *J. Exp. Biol.* **204**, 3587–3600.

Biewener, A. A. (1998). Muscle function *in vivo*: A comparison of muscles used for elastic energy savings *versus* muscles used to generate mechanical power. *Am. Zool.* **38**, 703–717.

Biewener, A. A., Corning, W. R. and Tobalske, B. W. (1998). *In vivo* pectoralis muscle force–length behaviour during level flight in pigeons (*Columba livia*). *J. Exp. Biol.* **201**, 3293–3307.

Biewener, A. A., Dial, K. P. and Goslow, G. E. (1992). Pectoralis muscle force and power output during flight in the starling. *J. Exp. Biol.* **164**, 1–18.

Casey, T. M. and Ellington, C. P. (1989). Energetics of insect flight. In *Energy Transformation in Cells and Organisms* (ed. W. Wieser and E. Gnaiger), pp. 200–210. Stuttgart: Georg Thieme Verlag.

Chai, P., Chen, J. S. C. and Dudley, R. (1997). Transient hovering performance of hummingbirds under conditions of maximal loading. *J. Exp. Biol.* **200**, 921–929.

Chai, P. and Dudley, R. (1995). Limits to vertebrate locomotor energetics suggested by hummingbirds hovering in heliox. *Nature* **377**, 722–725.

Chai, P. and Millard, D. (1997). Flight and size constraints: hovering performance of large hummingbirds under maximal loading. *J. Exp. Biol.* **200**, 2757–2763.

Cooper, A. J. (1993). Limitations of bumblebee flight performance. PhD thesis, University of Cambridge.

Dial, K. P. (1992). Avian forelimb muscles and nonsteady flight: can birds fly without using the muscles in their wings? *Auk* **109**, 874–885.

Dial, K. P. and Biewener, A. A. (1993). Pectoralis muscle force and power output during different modes of flight in pigeons (*Columba livia*). *J. Exp. Biol.* **176**, 31–54.

Dial, K. P., Biewener, A. A., Tobalske, B. W. and Warrick, D. R. (1997). Mechanical power output of bird flight. *Nature* **390**, 67–70.

Dudley, R. and DeVries, P. J. (1990). Flight physiology of migrating *Urania fulgens* (Uraniidae) moths: kinematics and aerodynamics of natural free flight. *J. Comp. Physiol. A* **167**, 145–154.

Earls, K. D. (2000). Kinematics and mechanics of ground take-off in the starling *Sturnis vulgaris* and the quail *Coturnix coturnix*. *J. Exp. Biol.* **203**, 725–739.

Ellington, C. P. (1984). The aerodynamics of hovering insect flight. VI. Lift and power requirements. *Phil. Trans. R. Soc. Lond. B* **305**, 145–181.

Ellington, C. P. (1991). Limitations on animal flight performance. *J. Exp. Biol.* **160**, 71–91.

Fisher, H. I. (1957). Bony mechanism of automatic flexion and extension in the pigeon's wing. *Science* **126**, 446.

Gans, C. and Gaunt, A. S. (1991). Muscle architecture in relation to function. *J. Biomech.* **24 (Suppl. 1)**, 53–65.

Garrod, A. H. (1875). On a point in the mechanism of the bird's wing. *Proc. Zool. Soc. Lond.* **1875**, 82–84.

George, J. C. and Berger, A. J. (1966). *Avian Myology*. New York: Academic Press. 108pp.

Girgenrath, M. and Marsh, R. L. (1999). Power of sound-producing muscles in the gray tree frogs *Hyla versicolor* and *Hyla chrysoscelis*. *J. Exp. Biol.* **202**, 3225–3237.

Griffiths, R. I. (1987). Ultrasound transit time gives direct measurement of muscle fibre length *in vivo*. *J. Neurosci. Meth.* **21**, 159–165.

Hartman, F. A. (1961). Locomotor mechanisms of birds. *Smithsonian Miscellaneous Collections* **143**, 1–91.

James, R. S., Cole, N. J., Davies, M. L. F. and Johnston, I. A. (1998). Scaling of intrinsic contractile properties and myofibrillar protein composition of fast muscle in the fish *Myoxocephalus scorpius* L. *J. Exp. Biol.* **201**, 901–912.

Josephson, R. K. (1985). Mechanical power output from striated muscle during cyclical contractions. *J. Exp. Biol.* **114**, 493–512.

Josephson, R. K., Malamud, J. G. and Stokes, D. R. (2000). Power output by an asynchronous flight muscle from a beetle. *J. Exp. Biol.* **203**, 2667–2689.

Kaiser, C. E. and George, J. C. (1973). Interrelationship amongst the avian orders Galliformes, Columbiformes and Anseriformes as evidenced by the fibre types in their pectoralis muscle. *Can. J. Zool.* **51**, 887–892.

Kiessling, K.-H. (1977). Muscle structure and function in the goose, quail, pheasant, guinea hen and chicken. *Comp. Biochem. Physiol.* **57B**, 287–292.

Marsh, R. L. (1994). Jumping ability of anuran amphibians. *Adv. Vet. Sci. Comp. Med.* **38B**, 51–111.

Marsh, R. L. (1999). How muscles deal with real-world loads: the influence of length trajectory on muscle performance. *J. Exp. Biol.* **202**, 3377–3385.

Marsh, R. L. and Olson, J. M. (1994). Power output of scallop adductor muscle during contractions replicating the *in vivo* mechanical cycle. *J. Exp. Biol.* **193**, 139–156.

Mathieu-Costello, O., Agey, P. J., Quintana, E. S., Rousey, K., Wu, L. and Bernstein, M. H. (1998). Fibre capillarization and ultrastructure of pigeon pectoralis muscle after cold acclimation. *J. Exp. Biol.* **201**, 3211–3220.

McGahan, J. (1973). Flapping flight of the Andean condor in nature. *J. Exp. Biol.* **58**, 239–253.

Norberg, U. M. (1975). Hovering flight in the pied flycatcher *Ficedula hypoleuca*. In *Swimming and Flying in Nature*, vol. 2 (ed. T. Y.-T. Wu, C. J. Brokaw and C. Boennnen), pp. 869–881. New York: Plenum Publishing Corp.

Norberg, U. M. (1976). Aerodynamics, kinematics and energetics of horizontal flapping flight in the long-eared bat *Plecotus auritus*. *J. Exp. Biol.* **65**, 179–212.

Norberg, U. M. (1990). *Vertebrate Flight: Mechanics, Physiology, Morphology, Ecology and Evolution*. Berlin: Springer-Verlag.

Norberg, U. M., Kunz, T. H., Steffensen, J. F., Winter, Y. and von Helversen, O. (1993). The cost of hovering and forward flight in a nectar-feeding bat, *Glossophaga soricinia*, estimated from aerodynamic theory. *J. Exp. Biol.* **182**, 207–227.

Pennycuick, C. J. (1968). Power requirements for horizontal flight in the pigeon *Columba livia*. *J. Exp. Biol.* **49**, 527–555.

Pennycuick, C. J. (1969). The mechanics of bird migration. *Ibis* **111**, 525–556.

Pennycuick, C. J. (1975). Mechanics of flight. In *Avian Biology*, vol. 5, chapter 1 (ed. D. S. Farner, J. R. King and K. C. Parkes), pp. 1–75. London: Academic Press.

Pennycuick, C. J., Fuller, M. R. and McAllister, L. (1989). Climbing performance of Harris' hawks (*Parabuteo unicinctus*) with added load: implications for muscle mechanics and for radiotracking. *J. Exp. Biol.* **142**, 17–29.

Pennycuick, C. J., Hedenström, A. and Rosén, M. (2000). Horizontal flight of a swallow (*Hirundo rustica*) observed in a wind tunnel, with a new method for directly measuring mechanical power. *J. Exp. Biol.* **203**, 1755–1765.

Pennycuick, C. J., Heine, C. E., Kirkpatrick, S. J. and Fuller, M. R. (1992). The profile drag coefficient of a Harris' hawk wing, measured by wake sampling in a wind tunnel. *J. Exp. Biol.* **165**, 1–19.

Pennycuick, C. J., Klaassen, M., Kvist, A. and Lindström, Å. (1996). Wingbeat frequency and the body drag anomaly: wind-tunnel observations on a thrush nightingale (*Luscinia luscinia*) and a teal (*Anas crecca*). *J. Exp. Biol.* **199**, 2757–2765.

Pennycuick, C. J., Obrecht, H. H. and Fuller, M. R. (1988). Empirical estimates of body drag of large waterfowl and raptors. *J. Exp. Biol.* **135**, 253–264.

Pennycuick, C. J. and Parker, G. A. (1966). Structural limitations on the power output of the pigeon's flight muscles. *J. Exp. Biol.* **45**, 489–498.

Peplowski, M. M. and Marsh, R. L. (1997). Work and power output in the hindlimb muscles of Cuban tree frogs *Osteopilus septentrionalis* during jumping. *J. Exp. Biol.* **200**, 2861–2870.

Rayner, J. M. V. (1979). A new approach to animal flight mechanics. *J. Exp. Biol.* **80**, 17–54.

Rayner, J. M. V. (1993). On aerodynamics and the energetics of vertebrate flapping flight. *Contemp. Math.* **141**, 351–400.

Rayner, J. M. V. (1995). Flight mechanics and constraints on flight performance. *Israel J. Zool.* **41**, 321–342.

Rayner, J. M. V. (1999). Estimating power curves of flying vertebrates. *J. Exp. Biol.* **202**, 3449–3461.

Rome, L. C., Sosniki, A. A. and Goble, D. O. (1990). Maximum velocity of shortening of three fibre types from horse soleus muscle: implications for scaling with body size. *J. Physiol., Lond.* **431**, 173–185.

Seow, C. Y. and Ford, L. E. (1991). Shortening velocity and power output of skinned muscle fibres from mammals having a 25,000-fold range of body mass. *J. Gen. Physiol.* **97**, 541–560.

Spedding, G. R. (1986). The wake of a jackdaw (*Corvus monedula*) in slow flight. *J. Exp. Biol.* **125**, 287–307.

Spedding, G. R. (1987). The wake of a kestrel (*Falco tinnunculus*) in flapping flight. *J. Exp. Biol.* **127**, 45–57.

Spedding, G. R., Rayner, J. M. V. and Pennycuick, C. J. (1984). Momentum and energy in the wake of a pigeon (*Columba livia*) in slow flight. *J. Exp. Biol.* **111**, 81–102.

Stevenson, R. D. and Josephson, R. K. (1990). Effects of operating frequency and temperature on mechanical power output from moth flight muscle. *J. Exp. Biol.* **149**, 61–78.

Suarez, R. K., Lighton, J. R. B., Brown, G. S. and Mathieu-Costello, O. (1991). Mitochondrial respiration in hummingbird flight muscles. *Proc. Natl. Acad. Sci. USA* **88**, 4870–4873.

Tobalske, B. W. and Dial, K. P. (2000). Effects of body size on take-off flight performance in the Phasianidae (Aves). *J. Exp. Biol.* **203**, 3319–3332.

van den Berg, C. and Rayner, J. M. V. (1995). The moment of inertia of bird wings and the inertial power requirement for flapping flight. *J. Exp. Biol.* **198**, 1655–1664.

Wakeling, J. M. and Ellington, C. P. (1997a). Dragonfly flight. II. Velocities, accelerations and kinematics of flapping flight. *J. Exp. Biol.* **200**, 557–582.

Wakeling, J. M. and Ellington, C. P. (1997b). Dragonfly flight. III. Lift and power requirements. *J. Exp. Biol.* **200**, 583–600.

Wakeling, J. M. and Johnston, I. A. (1998). Muscle power output limits fast-start performance in fish. *J. Exp. Biol.* **201**, 1505–1526.

Weis-Fogh, T. (1972). Energetics of hovering flight in hummingbirds and in *Drosophila*. *J. Exp. Biol.* **56**, 79–104.

Wells, D. J. (1993). Muscle performance in hovering hummingbirds. *J. Exp. Biol.* **178**, 39–57.

Williamson, M. R., Dial, K. P. and Biewener, A. A. (2001). Pectoralis muscle performance during ascending and level flight in mallards (*Anas platyrhynchos*). *J. Exp. Biol.* **204**, 495–507.

Willmott, A. P. and Ellington, C. P. (1997). Mechanics of flight in the hawkmoth *Manduca sexta*. II. Aerodynamic sonsequences of kinematic and morphological variation. *J. Exp. Biol.* **200**, 2723–2745.